

**KINETIC AND MOLECULAR MODELING OF SELECTED TOBACCO ALKALOIDS  
IN MAINSTREAM CIGARETTE SMOKE**

**CAREN CHEBET KURGAT**

**A Thesis Submitted to Board of Postgraduate Studies in Partial Fulfilment of the  
Requirements for the Award of the of Master of Science Degree in Chemistry of  
Egerton University**

**EGERTON UNIVERSITY**

**NOVEMBER, 2016**

## DECLARATION AND RECOMMENDATION

### DECLARATION

This is my original work and has not been presented for examination for the award of a degree in any institution.

Signature: .....

Date: .....

Caren C. Kurgat

SM11/23544/14

### RECOMMENDATION

This research has been submitted for examination with our approval as the University supervisors.

Signature: .....

Date: .....

Dr. Joshua K. Kibet

Department of Chemistry

Egerton University

Signature: .....

Date: .....

Prof. Peter K. Cheplogoi

Department of Chemistry

Egerton University

## **COPYRIGHT**

© 2016 Caren Chebet

No part of this thesis may be reproduced, scanned, photocopied, stored in a retrievable system or transmitted in any form without the permission of Egerton University on behalf of the author.

## **DEDICATION**

It is with sincere regards that I dedicate this work to my loving parents Mr. and Mrs. Simon and Linah Kurgat, my siblings Gerald, Geraldine, Gertrude, Joan, and Faith.

## **ACKNOWLEDGEMENT**

I give thanks to God with whose grace this task has been successfully completed. I thank Egerton University especially the Department of Chemistry for providing the necessary support and facilities towards the success of this study. My sincere gratitude to my supervisors Dr. J. K. Kibet and Prof. P. K. Cheplogoi of Egerton University for giving me the opportunity to do this research and ensuring that everything was done right during my entire period as a student. I am truly honoured to have been their student. My parents, brothers, sisters and friends are greatly acknowledged for their prayers, financial and moral support throughout this research. My class mates; Josephate Bosire and Nicholas Rono are appreciated for standing with me throughout my entire period as a student at Egerton University. The Directorate of Research and Extension is greatly acknowledged for partially funding this work. I also acknowledge the National Commission for Science, Technology and Innovation (NACOSTI) for funding my project.

## ABSTRACT

Consensus of opinion in literature regarding tobacco use has shown that cigarette smoking can cause irreparable damage to the genetic material, cell injury, and the general respiratory landscape. The alkaloid family of tobacco has been implicated in a series of ailments including addiction, mental illnesses, psychological disorders, and mental deficits. Accordingly, this study describes the kinetic and molecular modelling of the major tobacco alkaloids in mainstream cigarette smoke; nicotine,  $\beta$ -nicotyrine, and 3,5-dimethyl-1-phenylpyrazole with the principal focus of understanding their energetics, their environmental fate, and the formation of intermediates considered harmful to tobacco users. Two commercial cigarette brands coded SM1 and ES1 were explored for the evolution of major tobacco alkaloids over a modest temperature range of 200 – 700 °C for a total pyrolysis time of 3 minutes using a tubular quartz reactor, typically in increments of 100 °C using nitrogen as the pyrolysis gas. The heating rate was  $\sim 20 \text{ }^\circ\text{C s}^{-1}$ . The pyrolysate was analysed using a Gas-Chromatography hyphenated to a mass spectrometer (GC-MS) fitted with a mass selective detector (MSD). Analysis of pyrolysate using GC-MS showed that nicotine was the major alkaloid in both cigarettes, reaching a maximum at  $\sim 400 \text{ }^\circ\text{C}$  ( $8.0 \times 10^8$  GC-Area counts) for ES1 cigarette and about  $2.7 \times 10^8$  GC-Area counts for SM1 cigarette (at 500 °C). Moreover,  $\beta$ -nicotyrine and 3, 5-dimethyl-1-phenylpyrazole were also detected in significant amounts. Chemissian computational code was used to generate the electron density contour maps in order to determine the nucleophilicity of these alkaloids in relation to how they interact with biological molecules to cause toxicity and cell impairment. The density functional theory calculations were conducted with B3LYP correlation function and established that the scission of the phenyl C-C bond in nicotine and  $\beta$ -nicotyrine, and C-N phenyl bond in 3,5-dimethyl-1-phenylpyrazole were respectively 365.33, 507.37, and 494.24  $\text{kJmol}^{-1}$ . Clearly, the value of the bond dissociation energy is dependent on the  $\pi - \pi$  interactions which play a primary role in stabilizing the phenyl bonds. A kinetic model on the destruction of nicotine was proposed using pseudo-first order rate law and found that the rate constant  $k_1$  for the destruction of nicotine at 673 K was  $0.31\text{s}^{-1}$  and  $0.74 \text{ s}^{-1}$  for ES1 and SM1 cigarettes respectively. It was noted that the rate constant for the destruction of nicotine in SM1 is  $\sim 2$  times the rate constant for the destruction of nicotine in ES1. Based on nicotine information obtained from this study, it is clear that ES1 cigarette is more addictive than SM1 cigarette.

## TABLE OF CONTENTS

<b>DECLARATION AND RECOMMENDATION .....</b>	<b>ii</b>
<b>COPYRIGHT .....</b>	<b>iii</b>
<b>DEDICATION.....</b>	<b>iv</b>
<b>ACKNOWLEDGEMENT.....</b>	<b>v</b>
<b>ABSTRACT.....</b>	<b>vi</b>
<b>TABLE OF CONTENTS .....</b>	<b>vii</b>
<b>LIST OF TABLES .....</b>	<b>x</b>
<b>LIST OF FIGURES .....</b>	<b>xi</b>
<b>LIST OF SCHEMES .....</b>	<b>xiii</b>
<b>LIST OF APPENDICES .....</b>	<b>xiv</b>
<b>LIST OF ABBREVIATIONS AND ACRONYMS .....</b>	<b>xv</b>
<b>CHAPTER ONE .....</b>	<b>1</b>
<b>INTRODUCTION.....</b>	<b>1</b>
1.1 Background information .....	1
1.2 Computational chemistry .....	3
1.3 Statement of the problem .....	5
1.4 Objectives .....	6
1.4.1 General objective .....	6
1.4.2 Specific objectives .....	6
1.5 Hypotheses .....	6
1.6 Justification .....	6
<b>CHAPTER TWO .....</b>	<b>8</b>
<b>LITERATURE REVIEW .....</b>	<b>8</b>
2.1 Tobacco pyrolysis .....	8
2.2 Cigarette smoking .....	8
2.3 Nicotine.....	9

2.4 $\beta$ -nicotyrine and 3,5-dimethyl-1-phenylpyrazole.....	12
2.5 The formation kinetics of nicotine .....	13
2.6 Computational chemistry and molecular modeling .....	14
2.6.1 The density functional theory (DFT).....	15
2.6.2 Chemissian software.....	17
<b>CHAPTER THREE.....</b>	<b>18</b>
<b>MATERIALS AND METHODS .....</b>	<b>18</b>
3.1 Reagents and materials.....	18
3.2 Equipment, instruments, and computational softwares.....	18
3.3 Sample preparation.....	18
3.4 GC- MS characterization of molecular products.....	19
3.5 GC-MS analysis Quality Control (QC).....	19
3.6 Pyrolysis of tobacco .....	20
3.7 Computational methodology .....	20
3.8 The development of the kinetic model for the formation and destruction of nicotine...21	
<b>CHAPTER FOUR.....</b>	<b>25</b>
<b>RESULTS AND DISCUSSION .....</b>	<b>25</b>
4.1 Choice of basis set used in computational calculations .....	25
4.2 GC-MS characterization of selected alkaloids .....	26
4.3 Product distribution of nicotine in ES1 and SM1 cigarettes .....	27
4.4 Mechanistic pathways for radical formation and other possible molecular products ....29	
4.4.1 Proposed mechanistic channel for the thermal degradation of nicotine .....	29
4.4.2 Mechanistic description for the thermal degradation of $\beta$ -nicotyrine .....	31
4.4.3 The proposed mechanistic pathway for the thermal degradation of 3, 5-dimethyl-1-phenylpyrazole .....	32
4.5 Computational modeling of the selected alkaloids .....	35
4.5.1 Molecular geometries of major alkaloids .....	35

4.5.2 Molecular orbitals and electron density maps of nicotine.....	36
4.6 Decomposition profile of tobacco .....	40
4.7 The formation and destruction kinetics of nicotine.....	41
4.8 The proposed mechanistic pathways for the destruction of nicotine .....	44
4.9 Toxicological implications of molecular products from cigarette smoke.....	44
<b>CHAPTER FIVE .....</b>	<b>47</b>
<b>CONCLUSION AND RECOMMENDATIONS.....</b>	<b>47</b>
5.1 Conclusion.....	47
5.2 Recommendations .....	48
<b>REFERENCES.....</b>	<b>49</b>
<b>APPENDICES .....</b>	<b>59</b>

## LIST OF TABLES

Table 4.1: HOMO-LUMO band gap energies for the selected alkaloids under study.....	37
Table 4.2: The Arrhenius parameters for the destruction of nicotine from the pyrolysis of two commercial cigarettes (ES1 and SM1).....	42

## LIST OF FIGURES

Figure 1.1: Tobacco plantation.....	3
Figure 1.2: Graphical abstract of the major chemistry reported in this study.....	5
Figure 2.1: Molecular structure of nicotine.....	10
Figure 2.2: Molecular structure of $\beta$ -nicotyrine.....	13
Figure 2.3: Molecular structure of $\beta$ -nicotyrine.....	13
Figure 3.1: Apparatus set up for trapping cigarette smoke from cigarette burning.....	19
Figure 3.2: The relationship between the rates of formation of the intermediate product ( $R_f$ ) vs. the rate of destruction ( $R_d$ ) and $C_0$ the maximum concentration of the reaction product.....	21
Figure 4.1: A plot of enthalpy change for reactions 1-3 (scheme 4.1) at various basis sets.....	26
Figure 4.2: Overlay chromatograms for ES1 (red line) and SM1 (blue line) at 300 °C.....	27
Figure 4.3: Product distribution of nicotine and the selected alkaloids in mainstream cigarette smoke determined from the burning of two commercial cigarettes; ES1 (left) and SM1 (right).....	28
Figure 4.4: Product yields of $\beta$ -nicotyrine and 3, 5-dimethyl-1-phenylpyrazole (3, 5-dmpp) for ES1 cigarette (yellow) and SM1 (purple).....	28
Figure 4.5: Product distribution of pyridine and 3-methylpyridine in mainstream cigarette smoke determined from the burning of commercial cigarettes; ES1 (left) and SM1 (right).....	30
Figure 4.6: Product distribution of toluene and benzene in mainstream cigarette smoke determined from the burning of commercial cigarettes; ES1 (left) and SM1 (right).....	34

Figure 4.7: Optimized structure of nicotine and a plot showing its optimization steps (the red circle is the optimization level).....	35
Figure 4.8: Optimized structure of $\beta$ -nicotyrine and a plot showing its optimization steps (the red circle is the optimization level).....	35
Figure 4.9: Optimized structure of 3,5-dimethyl-1-phenylpyrazole and a plot showing its optimization steps (the red circle is the optimization level).....	36
Figure 4.10: The HOMO-LUMO band gap for nicotine determined using Chemissian.....	38
Figure 4.11: 2-D electron density map for nicotine.....	39
Figure 4.12: 3-D molecular orbital diagram showing electronic density for nicotine at an isovalue of 0.02.....	39
Figure 4.13: 1-D line showing the probability of finding electrons at a distance r from nicotine nuclei.....	40
Figure 4.14: Percentage (%) yield of char from tobacco.....	41
Figure 4.15: Formation kinetics of nicotine.....	42
Figure 4.16: Arrhenius plots for the destruction kinetics of nicotine in ES1 and SM1 cigarettes .....	43

## LIST OF SCHEMES

Scheme 4.1: The formation of various radicals from the thermal degradation of nicotine.....	25
Scheme 4.2: Proposed mechanistic pathways for the thermal degradation of nicotine.....	31
Scheme 4.3: Proposed mechanistic pathways for the thermal degradation of $\beta$ -nicotyrine.....	32
Scheme 4.4: Proposed mechanistic pathways for the thermal degradation of 3, 5-dimethyl-1-phenylpyrazole.....	33
Scheme 4.5: Mechanistic destruction of nicotine to radical intermediates and possible by-products.....	44

## LIST OF APPENDICES

Appendix 1A: 2-D electron density contour map for $\beta$ -nicotyrine.....	56
Appendix 1B: 3-D electron density map for $\beta$ -nicotyrine.....	57
Appendix 1C: Molecular orbital diagram for $\beta$ -nicotyrine.....	58
Appendix 2A: 2-D electron density contour map for 3, 5-dimethyl-1-phenylpyrazole.....	59
Appendix 2B: 3-D electron density map for 3, 5-dimethyl-1-phenylpyrazole.....	60
Appendix 2C: Molecular orbital diagram for 3, 5-dimethyl-1-phenylpyrazole.....	61
Appendix 3: Frequency and thermochemistry output file for optimization of pyridinyl radical.....	62
Appendix 4A: Molecular orbital diagrams for nicotine.....	68
Appendix 4B: Molecular orbital diagrams for $\beta$ -nicotyrine.....	69
Appendix 4C: Molecular orbital diagrams for 3,5-dimethyl-1-phenylpyrazole.....	70
Appendix 5A: MS-Fragmentation pattern of nicotine using Electron Impact Ionization (EI).....	71
Appendix 5B: MS-Fragmentation pattern of $\beta$ -nicotyrine using Electron Impact Ionization (EI).....	72

## LIST OF ABBREVIATIONS AND ACRONYMS

BAT	British American Tobacco
CVD	Cardiovascular Disease
COPD	Chronic Obstructive Pulmonary Disease
DALYs	Disability-adjusted life years
DFT	Density Functional Theory
DNA	Deoxyribonucleic acid
ES1	Cigarette 1
GC-MS	Gas chromatography – Mass spectrometry
HF	Hatree – Fock
HOMO	Highest occupied molecular orbital
HPLC	High Performance Liquid Chromatography
LUMO	Lowest unoccupied molecular orbital
MSD	Mass Selective Detector
NIST	National Institute of Standards and Technology
PES	Potential Energy Surface
pK <sub>a</sub>	Acid dissociation constant
QSAR	Quantitative Structural Activity Relationship
SM1	Cigarette 2
ZPVE	Zero-point vibrational energy

# CHAPTER ONE

## INTRODUCTION

### 1.1 Background information

There is substantial evidence to believe that inhaled toxicants such as cigarette smoke can cause irreparable damage to the genetic make-up, cell injury, and general respiratory landscape. Cigarette smoking continues to claim so many lives despite intense research in this area. Formation and emission of toxic by-products from tobacco at various smoking temperatures are a major health concern due to the associated health diseases; cardiac arrest, stroke, mental illnesses, and lung cancer. This is because the thermal degradation of complex plant materials such as tobacco gives rise to a variety of toxic substances including alkaloids such as nicotine,  $\beta$ -nicotyrine and 3, 5-dimethyl-1-phenylpyrazole. It is well established that the tobacco plant comprises 6-15% cellulose, 10-15% pectin, about 2% lignin, and many other components; the true composition being dependent on the tobacco plant type and growing conditions (Feng *et al.*, 2004). Tobacco consists of more than 2500 chemical constituents, including biopolymers, non-polymeric and inorganic compounds, and is believed to be one of the most poisonous plants especially owing to its use in the form of cigarettes (Czégény *et al.*, 2009). Sugars such as cellulose, pectin, alginates, laminarin, and ethyl cellulose are natural tobacco components which are often added to tobacco during the manufacturing process (Talhout *et al.*, 2006; Baker, 2007). Documentation of tobacco use as powder, chewing, smoking and sniffing dates back to its use by Native Americans in the 15<sup>th</sup> century (Christen *et al.*, 1982).

Tobacco alkaloids for instance nicotine from cigarette smoking has been known to cause significant environmental risks as well as cognitive problems for developing foetus (Hetch, 2012). Generally, nicotine in mainstream cigarette smoke exists in the particulate phase (Hecht, 2005; Siegel *et al.*, 2012). Furthermore, nicotine mimics certain actions of the neurotransmitter acetylcholine and it produces its discriminative stimulus effect in the hippocampus portion of the brain (Lockman *et al.*, 2005). The addictive properties of nicotine stem from its binding to nicotinic acetylcholine receptors (Zhou *et al.*, 2011). Nonetheless, nicotine is a primary substance in cigarette smoke that strongly affects brain development (Lisko *et al.*, 2013). Research on animals support biological evidence for increased motor action, neuro-behavioural, learning and memory deterioration, and change in neurotransmitter

function due to nicotine uptake (Kulshreshtha and Moldoveanu, 2003; Sharma *et al.*, 2004; Cho *et al.*, 2013).

Cigarettes, cigars and pipe tobacco are made from dried tobacco leaves and ingredients added for flavour and to make smoking more pleasant. The smoke from these products is a complex mixture of chemicals, including over 70 known to cause cancer. Some of the chemicals found in tobacco smoke include: cyanide, benzene, formaldehyde, methanol, acetylene and ammonia (Stedman, 1968). Tobacco alkaloids and especially nicotine sustains tobacco addiction, which in turn causes devastating health problems including heart diseases, lung diseases, and cancer (Benowitz, 2008). Tobacco use increases the risk of developing at least 14 types of cancer. It also accounts for about 25–30% of all deaths from cancer and 87% of deaths from lung cancer. Compared with non-smokers, male smokers are 23 times and female smokers 17 times more likely to develop lung cancer (Anand *et al.*, 2008). The formation and emission of potentially toxic by-products from tobacco at various combustion temperatures is therefore a major health concern due to associated health diseases such as heart attack, stroke and cardiovascular death, mental illnesses and lung cancer. Other areas of health concern arising from consumption of tobacco include effects on reproductive health for example blue babies, erectile dysfunction and mutagenicity.

Considering the intricate chemical nature of tobacco smoke with more than 7000 identified constituents and biological variety typified by the presence of carcinogens, toxicants, irritants, tumour promoters, co-carcinogens and inflammatory agents, any effort to identify individual compounds which cause lung cancer in smokers is difficult (Hetch, 2012). Inhalation studies of cigarettes smoke may have many consequences which may have been previously summarized, all relating to the fact that laboratory animals do not voluntarily inhale cigarette smoke but rather try to avoid it (Siegel *et al.*, 2012). Nevertheless, a number of relatively recent studies have demonstrated lung tumours induction in both rats and mice exposed to cigarette smoke and in the older literature, tumours of the hamster larynx were produced (Hecht, 2005).

Generally, tobacco use has always been a controversial subject with its increasing popularity on one side and the giving of evidence of health risks on the other. This investigation therefore is necessary not only in unraveling the evolution characteristics of the major alkaloids in tobacco in a wide range of pyrolysis temperatures but also in exploring the

nucleophilicity of these alkaloids towards biological molecules such as DNA, ribonucleic acid, and microsomes. Tobacco plantations (Figure 1.1) in Kenya are found mainly in Migori, Kuria, Meru, and parts of central province.



**Figure 1.1:** Tobacco plantation

The concept of tobacco development, composition and toxicity is a very rich area of study. In recent years a lot of effort has been devoted to the evaluation of the by-products of tobacco burning and the potency of cigarette smoking (Zhou *et al.*, 2011). However, the shortfalls in describing the toxic compound formation mechanism during tobacco burning and the challenges of developing model compounds which can burn under conditions that simulate actual cigarette smoking with respect to heating rate, temperature distribution, variation in oxygen concentration and residence time impede this undertaking (Schlotzhauer, 1982).

## 1.2 Computational chemistry

The foundation of computational chemistry is the conventional Schrödinger wave equation expressed by equation 1.1:

$$H\psi = E\psi \quad 1.1$$

where  $H$  is the Hamiltonian operator,  $\psi$  is the wave function (Eigen function of the Hamiltonian) and  $E$  is the total energy of the system (eigenvalue in the equation) (McQuarrie and Simon, 1997). The wave function describes the system and takes as variables the positions of electrons in the system leading to the global equation 1.2 below.

$$H \psi(\vec{r}_1, \dots, \vec{r}_N) = E \psi(\vec{r}_1, \dots, \vec{r}_N) \quad 1.2$$

whereas  $\vec{r}$  describes the position of the electron in space,  $\psi$  allows the properties of the system to be deduced. The wave function can be orthogonal or orthonormal over all space depending on conditions of the wave function (McQuarrie and Simon, 1997). Consider equation 1.3, *vide infra*.

$$\langle \psi_i / \psi_j \rangle = \delta_{ij} \begin{cases} 1 \text{ if } i = j \\ 0 \text{ if } i \neq j \end{cases} \quad 1.3$$

in quantum mechanics,  $\delta_{ij}$  is called the *Kronecker delta*.

Computational chemistry refers to a branch of chemistry utilizing computer simulation algorithms in solving chemical problems (McQuarrie and Simon, 1997). This is achieved by incorporating sufficiently well-developed methods of theoretical chemistry into effective computer programs, thereby allowing calculation of structures and properties of both molecules and solids. Whereas computational results are complementary to the information obtained by experimental methods, in some instances it has proved capable of predicting unobserved chemical phenomena (Ochterski, 2000). Furthermore the use of computational techniques currently plays a vital role in preliminary feasibility stages of most scientific research. For instance in nanotechnology, computational modeling has become an important characterization tool due to the difficulty of dealing with nano-sized materials. The application of high performance computing to such disciplines e.g. simulation (molecular modelling) has evidently reduced research time and cost. More importantly it eliminates the challenge of limited resources during research study in addition to the fact that it is comparatively safe and can be performed on many chemical systems. This tremendous growth and development within the application of molecular modeling can be attributed to increasing computing power facilitated by advances in hardware and software witnessed over the past decade. Powerful computational softwares with modern GUI-graphical user

interfaces e.g. Mathematica, NWchem, Spartan, Hyperchem, MatLab, Odyssey or Gaussian are now accessible. Quantum mechanical calculations simply offer mathematical description of the behaviour of electrons. However, the quantum mechanical equations have never been solved exactly for any chemical system apart from that of the hydrogen atom (Osorio *et al.*, 2013). Hence, computational chemistry is wholly founded on approximate solutions, some of which are more accurate than any known experimental data (Young, 2001).

The graphical illustration shown schematically in Figure 1.2 summarizes the chemistry discussed in this study; pyrolysis of tobacco, analysis of tobacco smoke products using a GC-MS analytical technique, kinetics of the thermal degradation of reaction products, and computational modelling of tobacco by-products.

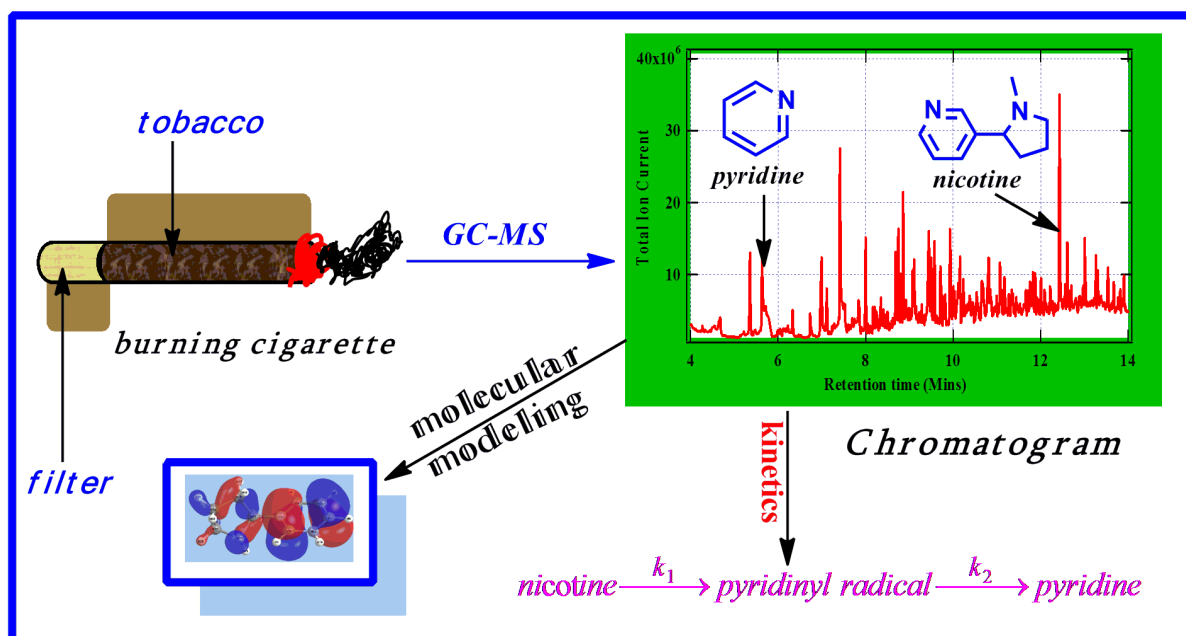


**Figure 1.2:** Graphical abstract of the major chemistry reported in this study

### 1.3 Statement of the problem

While nicotine is the most abundant alkaloid in tobacco, accounting for approximately 95% of alkaloid content, the minor alkaloids have been shown to exhibit biological activity in animals and may cause serious health consequences in humans than earlier thought. Minor tobacco alkaloids have been characterized to a lesser extent in tobacco but are believed to be carcinogenic and are linked to accidental poisoning and fatality in a few cases. This study therefore explored experimentally the temperature dependent evolution of minor tobacco alkaloids ( $\beta$ -nicotyrine and 3, 5-dimethyl-1-phenylpyrazole) which have received little attention in literature. Moreover, the kinetic and molecular modelling of tobacco alkaloids

was investigated in this study using Chemissian and the Density Functional Theory quantum analytical gradient with a view to understand their reactivity and toxicity towards biological structures.

## **1.4 Objectives**

### **1.4.1 General objective**

To explore the kinetic, mechanistic, and molecular modeling of selected tobacco alkaloids evolved in mainstream cigarette smoking.

### **1.4.2 Specific objectives**

1. To identify selected tobacco alkaloids (nicotine,  $\beta$ -nicotyrine, 3, 5 –dimethyl-1-phenylpyrazole) and to compare the concentration of nicotine in two commercial cigarettes SM1 and ES1 in mainstream cigarette smoking.
2. To propose a mechanistic degradation of nicotine,  $\beta$ -nicotyrine, 3, 5 –dimethyl-1-phenylpyrazole to intermediate free radicals.
3. To compute optimized molecular orbital geometries for nicotine,  $\beta$ -nicotyrine, 3, 5-dimethyl-1-phenylpyrazole using Gaussian and Chemissian computational softwares.
4. To determine the activation energy from the destruction kinetics of nicotine in mainstream cigarette smoke.

## **1.5 Hypotheses**

1. The concentration of nicotine in SM1 cigarette and ES1 cigarette are not the same in mainstream cigarette smoking.
2. The mechanistic degradation of nicotine,  $\beta$ -nicotyrine, 3,5 –dimethyl-1-phenylpyrazole will not yield the same intermediate free radicals
3. Molecular orbital optimized geometries of nicotine,  $\beta$ -nicotyrine, 3, 5-dimethyl-1-phenylpyrazole generated using Chemissian will be different from those generated using Gaussian computational software.
4. The activation energy for the kinetic destruction of nicotine used in mainstream cigarette smoking will not be the same for the two cigarettes (SM1 and ES1)

## **1.6 Justification**

Whereas many efforts have been engaged towards understanding the pyrolytic behaviour of tobacco, many complex and uncertain reaction processes are yet to be understood. The

identification of pyridine like components of tobacco using experimental methods such as Gas-Chromatography and High Performance Liquid Chromatography (HPLC) has proved markedly difficult. Therefore, computational methods with complementary experimental techniques including mass spectrometry coupled to a mass selective detector (MSD) which simulate the burning conditions in cigarette smoke are indispensable. Additionally, the use of computational techniques has proven useful in determining parameters that are not easily accessible using experimental methods. For instance, the electron density maps, band-gap energies, bond lengths, bond angles and toxicity indices of molecules can be generated using computational methods within shorter time scales thus saving research time and related costs.

## **CHAPTER TWO**

### **LITERATURE REVIEW**

#### **2.1 Tobacco pyrolysis**

Tobacco smoke is a highly dynamic and very complex matrix consisting of over 7000 compounds which makes a cigarette behave like a chemical reactor where several complex chemical processes take place during pyrolysis (Baker, 2006; Czégény *et al.*, 2009; Adam *et al.*, 2010; Forster *et al.*, 2015). Pyrolysis can be described as the direct decomposition of an organic matrix such as tobacco to obtain an array of reaction products in limited oxygen. The basic phenomena that occur during the thermal degradation of tobacco is the initiation of pyrolysis reactions which results in the release of organic volatiles and the formation of char (Babu, 2008). Thermal degradation reaction mechanisms are complex and therefore it is necessary to simplify pyrolysis parameters and physical properties in order to simulate the overall characteristics of biomass burning including tobacco (White *et al.*, 2011; Huang *et al.*, 2011). Pyrolysis experiments offer the possibility of unravelling mechanistic information about the complex processes involved in the thermal decomposition of tobacco biomass. Moreover, tobacco biomass in the form of cigarettes generates various smoke compounds during pyrolysis reactions (Mitschke *et al.*, 2005; Baker, 2007; Busch *et al.*, 2012).

#### **2.2 Cigarette smoking**

Cigarette smoking is an old age addictive habit that has attracted serious condemnation because of the clinical implications associated with it (Mitschke *et al.*, 2005; Busch *et al.*, 2012). Cigarette smoking causes serious health, economic, and social problems throughout the world (William *et al.*, 2012). Smoking has major adverse effects on almost every organ system in the body, accounting for more than 10% of deaths from all causes and 30% of deaths from cancer worldwide (Anand *et al.*, 2008). According to the Global Burden of Disease study, smoking causes tremendous disability, estimated at 2,276 disability-adjusted life years (DALYs) per 100,000 (Wang *et al.*, 2015). Smoking cessation, however, is extremely difficult because of the highly addictive nature of nicotine (Mendelsohn, 2011). Among regular smokers, withdrawal symptoms occur within two hours of the last cigarette, peaking within 24–48 hours and sometimes lasting for weeks or months (Abrams and Niaura, 2003).

The symptoms of cigarette withdrawal include cigarette craving, depression, insomnia, irritability, nervousness, anxiety, difficulty concentrating, restlessness and weight gain (Cappelleri *et al.*, 2005). Most smokers who quit smoking experience nicotine withdrawal symptoms due to their nicotine dependence (Benowitz, 2008). Usually the symptoms are most severe during the first 3 days following cessation but may continue for weeks (Shiffman *et al.*, 2006). The severity of these symptoms depends on the number of cigarettes smoked daily and duration of usage (Anderson *et al.*, 2002). It has also been shown that women are less successful in quitting smoking than men (Wetter *et al.*, 1999). Nicotine withdrawal symptoms are more severe in women and nicotine replacement therapy is less effective in them (Hesami *et al.*, 2010).

Smoking is the leading cause of preventable death (Pérez *et al.*, 2009). It has been estimated that tobacco smoking causes about 400,000 premature deaths per year in the United States, and approximately 4.9 million deaths per year worldwide (Foulds *et al.*, 2008). In Kenya, 69 per 100,000 deaths for individuals aged 30 and above are as a result of tobacco use. Five percent of all non-communicable deaths result from tobacco use, and 55% of all deaths from cancers of the trachea, bronchitis, and lung are attributable to tobacco (Mwenda *et al.*, 2015). Current trends show that tobacco use may cause more than 8 million deaths annually by 2030 (W.H.O, 2011). On average, smokers die 10 years earlier than non-smokers (Jha *et al.*, 2013). Alkaloids play a very important role in the sensory properties of tobacco smoke (Kulshreshtha and Moldoveanu, 2003).

### **2.3 Nicotine**

Nicotine (Figure 2.1) is a natural ingredient acting as a botanical insecticide in tobacco leaves. It is the principal tobacco alkaloid, occurring to the extent of about 1.5% by weight in commercial cigarette tobacco and comprising about 95% of the total alkaloid content (Lisko *et al.*, 2013). Oral snuff and pipe tobacco contain concentrations of nicotine similar to cigarette tobacco, whereas cigar and chewing tobacco have only about half the nicotine concentration of cigarette tobacco (Cho *et al.*, 2013). An average tobacco rod contains 10–14 mg of nicotine, and on average about 1–1.5 mg of nicotine is absorbed systemically during smoking. Nicotine in tobacco is largely the levorotary (*S*)-isomer; only 0.1–0.6% of total nicotine content is (*R*)-nicotine. Chemical reagents and pharmaceutical formulations of (*S*)-nicotine have a similar content of (*R*)-nicotine (0.1–1.2%) as impurity since plant-derived nicotine is used for their manufacture (Benowitz *et al.*, 2009).

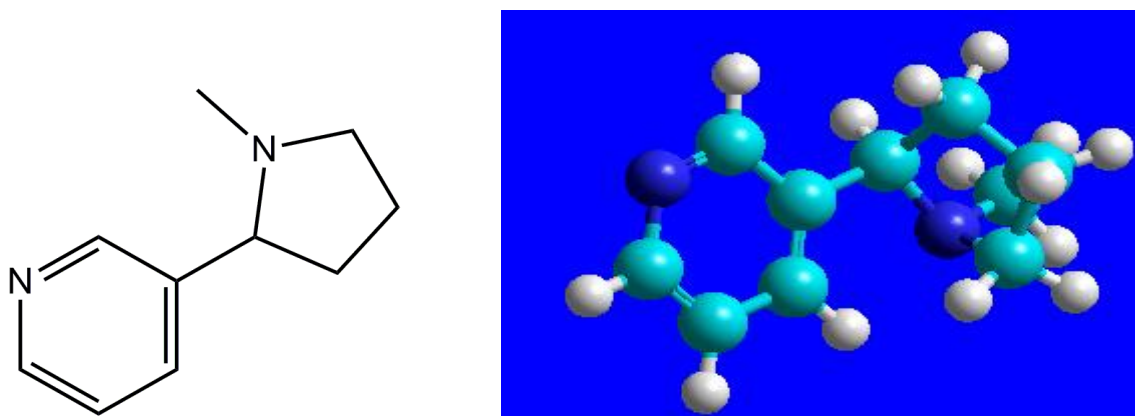


**Figure 2.1:** Molecular structure of nicotine: ChemDraw (left) and HyperChem modeling (right)

Nicotine is one of the more than 7000 chemicals found in the smoke from tobacco products; it is the primary content that acts on the brain (Benowitz, 2010). Nicotine is a naturally occurring colourless liquid that turns brown when burned and takes on the odour of tobacco when exposed to air. It can reach peak levels in the bloodstream and brain rapidly, depending on how it is taken. Cigarette smoking results in nicotine reaching the brain within just 10 seconds of inhalation (Leshner, 1998).

Nicotine mimics certain actions of the neurotransmitter, acetylcholine and it also appears to produce its discriminative stimulus effect in at least one major brain area, the hippocampus (Pomerleau and Rosecrans, 1989). The addictive properties of nicotine result from its binding to nicotinic acetylcholine receptors (Hetch, 2012). Moreover, nicotine is a key substance in cigarette smoke that strongly affects brain development (Zhao, Ford, Tsai, Li, Ahluwalia, Pearson, *et al.*, 2012).

Many aspects of the general pathways of carcinogenesis are firmly established but there are still some areas that could benefit from further investigation (Hecht, 2005; Duncan *et al.*, 2009). These include structural analysis of DNA adducts in smokers' lungs, a better understanding of the role of non-genotoxic tobacco smoke constituents in the lung cancer process, the role of polymorphisms in genes involved in nicotine and carcinogen uptake and metabolism, and the identification of smokers in danger of lung cancer (Shaywitz and Shaywitz, 1996). A better understanding of mechanisms of lung cancer initiation by cigarette

smoke can provide new insights on prevention of lung cancer in smokers, and possibly on cancer prevention (Hecht, 2005).

High prenatal nicotine exposure has a negative impact on reading performance in school age children. In addition, modeling has shown that environmental factors significantly moderated the interaction between prenatal nicotine exposure and reading skill outcomes (Cho *et al.*, 2013). Numerous investigations have explored the relationship between maternal smoking during pregnancy and various cognitive and behavioural disorders. Maternal smoking has been correlated with decreased performance on tests of intelligence, academic achievement, short-term and verbal working memory, long-term and immediate memory for auditory and verbal material, executive function, increased incidence of behavioural indices during childhood and adolescence, hyperactivity, and attention deficit disorders (Duncan *et al.*, 2009). Animal studies support biological evidence for accelerated motor activity, neurobehavioral, learning and memory deficits, and alteration of neurotransmitter function due to exposure to nicotine (Zhao, Ford, Tsai, Li, Ahluwalia and Pearson, 2012; Cho *et al.*, 2013).

Cigarette smoking exposes the developing foetus to nicotine and this may pose significant environmental risk factor for variability in reading skills (Duncan *et al.*, 2009). Nicotine also affects the cardiovascular system in many ways, that is by activating the sympathetic nervous system, nicotine induces increased heart rate and myocardial contraction, vasoconstriction in the skin and adrenal and neural release of catecholamine (Benowitz, 1996). Nicotine can also affect lipid metabolism (Cluette-Brown *et al.*, 1986), accelerate the development of atherosclerosis (Strohschneider *et al.*, 1994) and induce endothelial dysfunction (Chalon *et al.*, 2000). After entering the circulation, nicotine is subjected to extensive metabolism, resulting in a number of major and minor metabolites. On average, 70-80% of the nicotine is metabolized to cotinine; about 4% is converted to nicotine-1'-N-oxide and 0.4% to nornicotine (Benowitz and Jacob, 1994).

Cotinine is further metabolized to cotinine-N-oxide and trans-3'-hydroxycotinine, among others. Trans-3'-hydroxycotinine is the most abundant metabolite in urine, accounting for on average 38% of the metabolites (Benowitz, 2001). As most of the metabolites have a considerably longer physiological half-life compared to nicotine, plasma concentrations of nicotine metabolites in tobacco users tend to accumulate throughout the day (Ljungberg *et*

*al.*, 2013). Nicotine in mainstream cigarette smoke is primarily present in the particulate phase. Remarkably, however, the deposition efficiency of smoke particles in the respiratory tract is less effective than is the nicotine retention (Duncan *et al.*, 2009; Neha G. and Derek, 2010).

Absorption of nicotine across biological membranes depends on pH (Hukkanen *et al.*, 2005). Nicotine is a weak base with a  $pK_a$  of 8.0 (Robson *et al.*, 2010). In its ionized state, such as in acidic environments, nicotine does not rapidly cross membranes (Benowitz *et al.*, 2009). The  $pH$  of smoke from flue-cured tobaccos, found in most cigarettes, is acidic ( $pH$  5.5–6.0). At this  $pH$ , nicotine is primarily ionized. Therefore, there is little buccal absorption of nicotine from flue-cured tobacco smoke, even when it is held in the mouth (Gori *et al.*, 1986). Smoke from air-cured tobaccos, the predominant tobacco used in pipes, cigars, and some European cigarettes, is less acidic ( $pH$  6.5 or higher) and considerable nicotine is un-ionized (Benowitz, 1999). Smoke from these products is well absorbed through the mouth (Armitage *et al.*, 1978). It has recently been proposed that the  $pH$  of cigarette smoke particulate matter is higher than previously thought, and thus, a larger portion of nicotine would be in the un-ionized form, facilitating rapid pulmonary absorption (Pankow, 2001).

When tobacco smoke reaches the small airways and alveoli of the lung, nicotine is rapidly absorbed (Benowitz, 1988). Blood concentrations of nicotine rise quickly during a smoke and are at peak at the completion of smoking (Hukkanen *et al.*, 2005). The rapid absorption of nicotine from cigarette smoke through the lungs, is because of the huge surface area of the alveoli and small airways, and dissolution of nicotine in the fluid of  $pH$  7.4 in the human lung facilitates transfer across membranes (Benowitz *et al.*, 2009). After a puff, high levels of nicotine reach the brain in 10–20 s, faster than with intravenous administration, producing rapid behavioural reinforcement (Benowitz, 1990). The rapidity of rise in nicotine levels permits the smoker to titrate the level of nicotine and related effects during smoking, and makes smoking the most reinforcing and dependence-producing form of nicotine administration (Henningfield and Keenan, 1993).

#### **2.4 $\beta$ -nicotyrine and 3,5-dimethyl-1-phenylpyrazole**

These are considered minor alkaloid components of tobacco. Although their concentration in tobacco smoke may be low, their health impacts on biological and physiological systems could be devastating. It should nevertheless be noted that  $\beta$ -nicotyrine and 3, 5-dimethyl-1-

phenylpyrazole (Figures 2.2 and 2.3) are scarcely investigated in literature. Therefore, these critical molecular products of tobacco burning have largely been ignored in the past. Therefore, this study gives the first elaborate treatment on the evolution, thermochemical properties as well as the electronic characteristics of these alkaloids.  $\beta$ -nicotyrine is an established cancer causing agent derived from nicotine (Liu *et al.*, 2000).

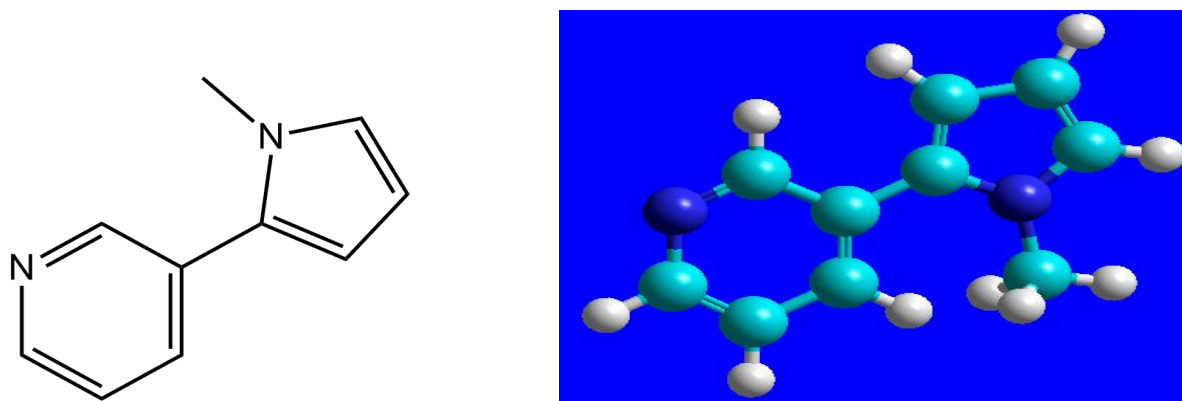


**Figure 2.2:** Molecular structures of  $\beta$ -nicotyrine: ChemDraw (left) and HyerChem modeling (right)

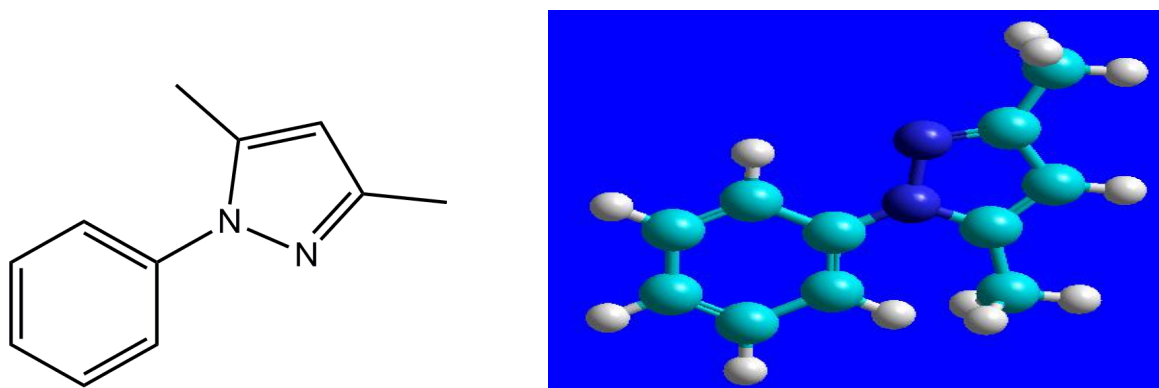


**Figure 2.3:** Molecular structures of 3,5-dimethyl-1-phenylpyrazole: ChemDraw (left) and HyerChem modeling (right)

## 2.5 The formation kinetics of nicotine

A global kinetic model was employed to obtain the kinetic parameters for the formation behaviour of nicotine (Taylor *et al.*, 1990). Pseudo-unimolecular rate law was applied in which the empirical rate of decomposition of the initial product was first order and expressed by equation 2.1.

$$C = C_o e^{-kt}$$

2.1

where:  $C_0$  is the concentration of the reactant (nicotine) at the peak of the curve while  $C$  is the concentration of the reactant at any temperature  $T$ , and  $k$  is the pseudo-unimolecular rate constant in the Arrhenius expression (cf. equation 2.2) at a residence time of 2.0 sec.

$$k = A e^{-\frac{E_a}{RT}} \quad 2.2$$

$A$  is the pre-exponential factor ( $s^{-1}$ ),  $E_a$  is the activation energy ( $\text{kJmol}^{-1}$ ),  $R$  is the universal gas constant ( $8.314 \text{ Jk}^{-1}\text{mol}^{-1}$ ), and  $T$  is the temperature in K.

The integrated form of the first order rate law (cf. equation 2.3) was used to calculate the rate constant for the pyrolysis behaviour of nicotine at three different reaction times; 2.0 and 5.0 and 10 seconds.

$$k = \ln\left(\frac{C_0}{C}\right) \times \frac{1}{t} \quad 2.3$$

The activation energy was determined from the Arrhenius plot ( $\ln k$  vs.  $\frac{1}{T}$ ) which establishes a linear relationship between the pre-exponential factor  $A$  and the rate constant  $k$  as given by equation 2.4, where  $\ln A$  is the y-intercept and  $-\frac{E_a}{RT}$  is the slope.

$$\ln k = \ln A - \frac{E_a}{RT} \quad 2.4$$

## 2.6 Computational chemistry and molecular modeling

The term computational chemistry is largely used when a mathematical technique is sufficiently well developed that it can be automated for operation on a computer. Molecular modeling is one of the most valuable and essential tools that are used by chemists in molecular design and it describe the generation, manipulation and representation of 3-dimensional structures (Nadendla, 2004). Computational techniques that are represented by molecular modeling usually play a critical role in the process of molecular design, which makes these computational techniques important steps of successful modeling procedures (Young, 2001). Quantum chemical calculations of thermodynamic data have developed beyond the level of simply reproducing experimental values, and can now make accurate predictions for molecules whose experimental data are unknown. The target is usually set as  $\pm 2 \text{ kcal mol}^{-1}$  for energy.

Scientists and engineers first got their hands on computers in the late 1960s and the growth in understanding and application of molecular modeling has run parallel with growth in computer power. The two greatest driving forces in recent years have been the personal computers (PCs) and the graphical user interface. At this time tremendously powerful molecular modelling computer packages such as Gaussian, HyperChem, Mopac and many more are commercially available, and the subject is routinely taught as part of undergraduate science degrees (Hinchliffe, 2005).

Quantum mechanics gives a mathematical account of the behaviour of electrons and has never been found to be wrong. However, the quantum mechanical equations have never been solved exactly for any chemical system other than the hydrogen atom. Thus, the entire field of computational chemistry is constructed around approximate solutions, some of which are more accurate than any known experimental data (Young, 2001; Osorio *et al.*, 2013). The molecular orbitals are represented by capital letters S, P, D, F, G, . . . consistent with the angular momentum quantum number  $L = 0, 1, 2, 3, 4, \dots$ , respectively. For a given quantum number  $L$ , the lowest shell orbital has the principal quantum number  $N = 1$  (Osorio *et al.*, 2013). A perfect sequence of phenomenological shell orbitals in a spherical potential is 1S, 1P, 1D, 2S, 1F, 2P, 1G, 2D, 3S, . . . However, the energy ordering of the shell orbitals and the degeneracies in sub-shells can be altered according to the potential, which depends on the details of the structural arrangement and the atomic charges. To calculate the energy change for formation of a compound or a radical from its constituents, the following thermodynamic equation 2.5 is employed (Ochterski, 2000; Frisch *et al.*, 2004).

$$\Delta_r H^0 = \sum (\varepsilon_0 - H_{corr})_{products} - \sum (\varepsilon_0 - H_{corr})_{reactants} \quad 2.5$$

where  $\Delta_r H^0$  is change in enthalpy of the reaction,  $H_{corr}$  is correction to the thermal enthalpy and  $\varepsilon_0$  is the sum of electronic and thermal enthalpies.

### 2.6.1 The density functional theory (DFT)

Most of the equations presented in this section are obtained from references (McQuarrie and Simon, 1997). DFT is a highly accurate computational method which can be considered an improvement of the Hartree-Fock (HF) theory where the many electron system of the electron correlation is modelled by a function of electron density. DFT is comparable to HF computationally but provides significantly better results and contains no approximations.

This computational method is exact. The electronic energy is written in the DFT application and expressed in terms of equation 2.6 (Ochterski, 2000; Frisch *et al.*, 2004):

$$\varepsilon_{el}[p] = \varepsilon_I[p] + \varepsilon_J[p] + \varepsilon_X[p] + \varepsilon_C[p] \quad 2.6$$

where the square brackets represent a functional of the one-electron density  $\rho(r)$ . The first term on the right-hand side gives the one-electron energy, the second term is the Coulomb contribution, the third term the exchange and the fourth term gives the correlation energy (McQuarrie and Simon, 1997).

In discussing the nature of various functionals, it is convenient to adopt some of the notation commonly used in the field. For instance, the functional dependence of  $E_{XC}$  on the electron density is expressed as an interaction between the electron density and an ‘energy density’  $\varepsilon_{XC}$  that is *dependent* on the electron density, equation 2.7.

$$E_{XC}[\rho(r)] = \int \rho(r) \varepsilon_{XC}[\rho(r)] dr \quad 2.7$$

The energy density  $\varepsilon_{XC}$  is always treated as a sum of individual exchange and correlation contributions. Within this formalism, it is clear that the Slater energy density is given by equation 2.8.

$$\varepsilon_X[\rho(r)] = -\frac{9\alpha}{\pi} \left(\frac{3}{\pi}\right)^{\frac{1}{3}} \rho^{\frac{1}{3}}(r) \quad 2.8$$

Another convention expresses the electron density in terms of an effective radius such that exactly one electron would be contained within the sphere defined by that radius were it to have the same density throughout as its centre. This behaviour is given by equation 2.9.

$$rS = \left(\frac{3}{4\pi\rho(r)}\right)^{\frac{1}{3}} \quad 2.9$$

In defining spin density the individual functionals of  $\alpha$  and  $\beta$  are used. The spin densities at any position are typically expressed in terms of  $\zeta$ , the normalized spin polarization as presented in equation 2.10.

$$\zeta(r) = \frac{\rho^\alpha(r) - \rho^\beta(r)}{\rho(r)} \quad 2.10$$

so that the  $\alpha$  spin density is simply one-half the product of the total  $\rho$  and  $(\zeta + 1)$ , and the  $\beta$  spin density is the difference between that value and the total  $\rho$ .

### 2.6.2 Chemissian software

Chemissian *ver.3.3* (Lenoid, 2012) is an analysing tool for molecules' electronic structure and spectra. It is used to develop molecular orbital energy-level diagrams (band-gap energies), experimental UV-Vis electronic spectra, natural transition orbitals and electronic and/or spin density maps. It has a user-friendly graphical interface and it can examine and visualize data from the output of US-Gamess, Firefly/PC-Gamess, Q-Chem, Spartan and other quantum chemical program packages. Chemissian tools also help to investigate nature of transitions in UV-Vis spectra and the bonding nature of molecules (Wójcik *et al.*, 2013). However, in this work, Chemissian will be used alongside Gaussian '09 computational suite of programs to generate molecular orbital energy levels, 3-D and 2-D electron density maps, and 1-D which defines the electronic probability within the nuclei which make up the molecular system.

## CHAPTER THREE

### MATERIALS AND METHODS

#### 3.1 Reagents and materials

All chemicals and reagents used in this study were of analytical grade (purity  $\geq 99\%$ ). Methanol was purchased from Sigma Aldrich Inc., St. Louis, Missouri, USA. Two commercial cigarette brands coded SM1 and ES1 were purchased from local retail outlets and used without further treatment.

#### 3.2 Equipment, instruments, and computational softwares

Agilent Technologies 7890A GC system connected to an Agilent Technologies 5975C (GC-MS) and a stopwatch were used in this work. Gaussian '09, HyperChem, and Chemissian *ver.3.3* computational softwares were used to compute geometry optimization of molecules, thermochemistry, and electron density contour maps of frontier orbitals of selected tobacco alkaloids.

#### 3.3 Sample preparation

Five (5) cigarette sticks were randomly selected from a pack of SM1 or ES1 cigarettes, weighed and smoked using the apparatus set up presented in Figure 3.1. All experiments were conducted in a fume chamber to minimize the health hazards associated with cigarette smoking. A cigarette stick was placed at the tip of tubing connected to a vacuum as shown in Figure 3.1 and lit with a match box. To sustain the burning of the cigarette, a syringe was used to draw in air to the burning cigarette. To prepare one sample, 5 cigarettes were smoked, implying that the alkaloid content reported in this study was an average of 5 cigarettes. The cigarettes were smoked using a syringe at a rate of 35 mL/s according to ISO 3402:1999 standards, and cigarette smoke collected in 50 mL analytical grade methanol. To investigate the formation kinetics of nicotine, the smoking process was timed using a stop watch at intervals of 2 seconds, 5 seconds, and 10 seconds in accordance with the common residence times in cigarette smoking. All samples were prepared in replicates in order to enhance reliability and reproducibility of data. The apparatus set for this investigation is presented in Figure 3.1.

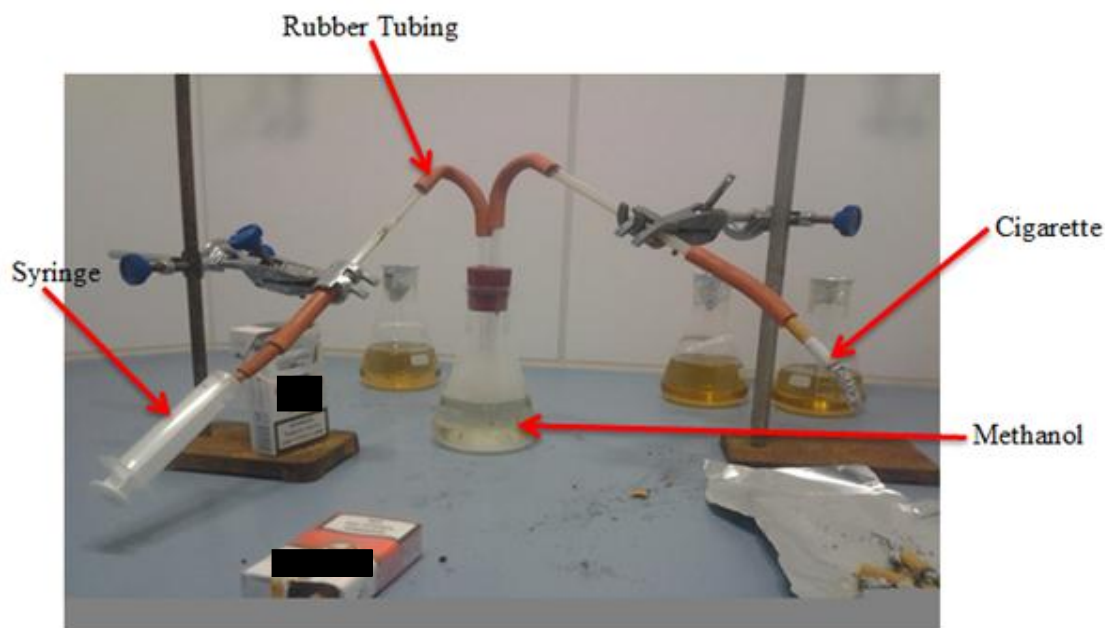


**Figure 3.1:** Apparatus set up for trapping cigarette smoke from cigarette burning

### 3.4 GC- MS characterization of molecular products

The quantitative analysis of nicotine,  $\beta$ -nicotyrine and 3,5-dimethyl-1-phenylpyrazole was carried out using an Agilent Technologies 7890A GC system connected to an Agilent Technologies 5975C inert XL Electron Ionization/Chemical Ionization (EI/CI) with a triple axis mass selective detector (MSD), using HP-5MS 5% phenyl methyl siloxane capillary column (30 m x 250  $\mu$ m x 0.25  $\mu$ m). The temperature of the injector port was set at 200  $^{\circ}$ C to vaporize the organic components for GC-MS analysis. The carrier gas was ultra-high pure (UHP) helium (99.999%). Temperature programming was applied at a heating rate of 15  $^{\circ}$ C for 10 minutes, holding for 1 minute at 200  $^{\circ}$ C followed by a heating rate of 25  $^{\circ}$ C for 4 minutes, and holding for 10 minutes at 300  $^{\circ}$ C. Electron impact ionization energy of 70 eV was used. To ensure that the right compounds were detected, standards were run through the GC-MS system and the peak shapes and retention times compared with those of nicotine,  $\beta$ -nicotyrine and 3,5-dimethyl-1-phenylpyrazole. The data was then run through the NIST library database as an additional tool to confirm the identity of compounds (Kibet *et al.*, 2012). Experimental results were averaged replicates of two experimental runs.

### 3.5 GC-MS analysis Quality Control (QC)

For accurate and consistent analysis, before any run was made, the mass spectrometer was tuned to check for leaks and water levels in the instrument which would affect the accuracy

of the data. This procedure was very important in order to prevent contamination, and extend the life of the EI filament. Quantitative transport tests were initiated before any run was conducted to ensure that there were no leaks in the GC-MS system and guarantee the pyrolysis system is clean. The flow rate in the transfer line was monitored to make sure that it was constant and did not fluctuate. If the flow rate was not consistent, and the pressure was not stable when the transfer line was connected to the GC-MS then leaks could be present in the system. This was corrected before any experiment could begin. To correct for any leaks in the system, a gas leak detector was used. Whenever leaks were detected along the gas lines, transfer lines, or reactor-injection port interface, the connections were tightened and quantitative transport experiment repeated to make sure no leaks were in the system. A known concentration of nicotine was injected into GC-MS system to monitor how much nicotine was recovered after analysis. This was to test the efficiency of the GC-MS instrument. A recovery of ~ 95% was good enough in order to proceed with analysis.

### **3.6 Pyrolysis of tobacco**

Tobacco of mass  $0.650 \pm 0.2$  g was weighed accurately into a crucible and carefully placed in a furnace. The tobacco in the furnace was then pyrolyzed at different temperatures; 200, 300, 400, 500, 600 and 700 °C at a constant pyrolysis time of 3 minutes to monitor the char yield of tobacco biomass. The data obtained in this study were averaged from two replicates. The residue formed at every pyrolysis temperature was collected and weighed in order to determine the yields of char.

### **3.7 Computational methodology**

All calculations were performed using the *Gaussian '09* computational program (Frisch *et al.*, 2009) . *Ab initio* calculations including correlation effects were made using the Density functional (DFT) level of theory with the 6-31G basis set. The frequency calculations also provide thermodynamic quantities such as zero-point vibrational energy (ZPVE), temperature corrections, and absolute entropies (Domingo *et al.*, 1997). The optimized geometries and molecular orbitals of molecular components were used in frequency calculations in order to determine their global energies and subsequently establish their global minima. Enthalpy changes were computed between the enthalpies of formation of the reactant (neutral compound) and its corresponding free radical. Chemissian *ver.3.3* (Lenoid, 2012) computational software was used to model molecular orbital energy level diagrams, electron

density maps as well as determine the band gap energies of frontier orbitals (HOMO-LUMO) for the selected tobacco alkaloids.

### 3.8 The development of the kinetic model for the formation and destruction of nicotine

In the development of the kinetic model of nicotine from the thermal degradation of tobacco biomass, fundamental assumptions were proposed: (1) the rate of formation of nicotine prevails the rate of destruction, (2) at the peak of the curve, the rates of formation and destruction are approximately the same, and (3) as the temperature is increased, the rate of destruction overwhelms the rate of formation. These assumptions were made based on the fact that pyrolysis of tobacco leads to the formation of nicotine, one of the major tobacco alkaloids as articulated in literature (Armitage *et al.*, 2004; Borgerding and Klus, 2005; Forster *et al.*, 2015). Therefore, from these assumptions, it was possible to calculate the apparent kinetic parameters for the destruction of nicotine from the temperature dependence of its yields.

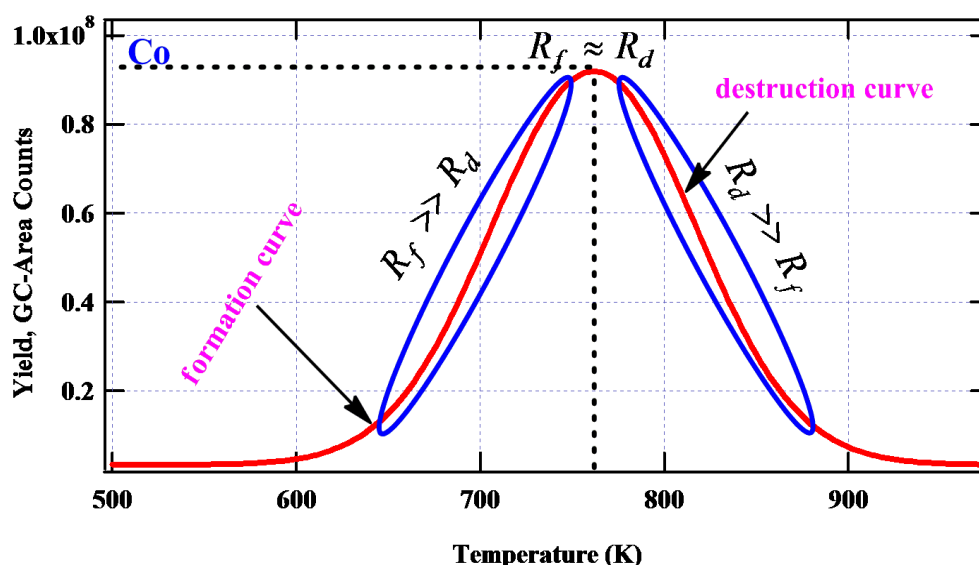


**Figure 3.2:** The relationship between the rates of formation of the intermediate product ( $R_f$ ) vs. the rate of destruction ( $R_d$ ) and  $C_0$  the maximum concentration of the reaction product

In this study, GC-Area counts were used to determine the destruction rate constants because according to the first order reaction kinetics (equations 3.3) the ratio of concentrations at various temperatures is a constant. Therefore, calibration of nicotine will still achieve comparable results.

The rate of formation of nicotine from the burning of tobacco was also determined experimentally at modest puff times (2, 5, and 10 seconds). For every puff time, the concentration of nicotine was determined using a GC-MS hyphenated to a mass selective detector (MSD). For simplicity, a consecutive first order reaction with rate constants  $k_1$  and  $k_2$  was considered in which a global kinetic model was employed to obtain the kinetic parameters for the thermal destruction of nicotine in mainstream cigarette smoking (Taylor *et al.*, 1990). Accordingly, pseudo-unimolecular reaction was applied in which the empirical rate of decomposition of the initial product is first order and expressed by equation 3.1.

$$C = C_o e^{-kt} \quad 3.1$$

where  $C_o$  is the concentration of the reactant (nicotine) at the peak of the curve while  $C$  is the concentration of the reactant at any temperature  $T$ , and  $k$  is the pseudo-unimolecular rate constant in the Arrhenius expression (cf. equation 3.2).

$$k = A e^{-\frac{Ea}{RT}} \quad 3.2$$

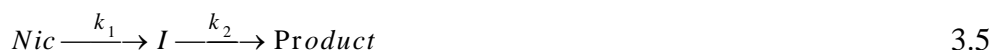
$A$  is the pre-exponential factor ( $s^{-1}$ ),  $Ea$  is the activation energy ( $kJmol^{-1}$ ),  $R$  is the universal gas constant ( $8.314 JK^{-1}mol^{-1}$ ), and  $T$  is the temperature in  $K$ . Despite all the criticisms against the Arrhenius rate law, it remains the only kinetic expression that can satisfactorily account for the temperature-dependent behaviour of even the most unconventional reactions including biomass pyrolysis (White *et al.*, 2011). The integrated form of the first order rate law (cf. equation 3.3) was used to calculate the rate constant for the pyrolysis behaviour of tobacco at a reaction time of 2.0 seconds. A reaction time of 2.0 seconds is universally used as the average time it takes for products to be formed in combustion systems (Nganai *et al.*, 2012). It is also considered as the standard residence time for the formation and destruction of reaction products in combustion processes (Kibet *et al.*, 2012).

$$k = \ln\left(\frac{C_o}{C}\right) \frac{1}{t} \quad 3.3$$

The activation energy was determined from the Arrhenius plots ( $\ln k$  vs.  $1/T$ ) which establishes a linear relationship between the pre-exponential factor  $A$  and the rate constant  $k$  as given by equation 3.4, where  $\ln A$  is the y-intercept and  $-\frac{Ea}{RT}$  is the slope.

$$\ln k = \ln A - \frac{Ea}{RT} \quad 3.4$$

The single step reaction mechanism below (equation 3.5) was considered during the thermal degradation of nicotine. Although tobacco pyrolysis is very complex, some understanding on the kinetic behaviour of certain reaction products from basic kinetic equations can be deduced. Therefore, this model was used based on relevant assumptions discussed under Figure 3.2.



Conventionally, the differential rate laws for each species  $Nic$  (nicotine),  $I$  (intermediate), and the final  $product$  are given by equations 3.6, 3.7, and 3.8 respectively

$$\frac{d[Nic]}{dt} = -k_1[Nic] \quad 3.6$$

$$\frac{d[I]}{dt} = k_1[Nic] - k_2[I] \quad 3.7$$

$$\frac{d[Product]}{dt} = k_2[I] \quad 3.8$$

These equations were solved analytically so that the integrated rate laws are expressed by equations 3.9 and 3.10.

$$[Nic] = [Nic]_0 e^{-k_1 t} \quad 3.9$$

Equations 3.10 and 3.11 give the respective concentrations of the intermediate  $I$  and the  $product$  at any time  $t$ .

$$[I] = \frac{k_1[Nic]_0}{k_2 - k_1} \left( e^{-k_1 t} - e^{-k_2 t} \right) \quad 3.10$$

$$[Product]_t = [Nic]_0 \left[ 1 + \frac{k_1}{k_1 - k_2} \left( k_2 e^{-k_1 t} - k_1 e^{-k_2 t} \right) \right] \quad 3.11$$

In order to simplify equation 3.11 further, it is assumed that step two (equation 3.5) is the rate determining step so that  $k_2 \ll k_1$  and thus the term  $e^{-k_1 t}$  decays more rapidly than the term

$e^{-k_2 t}$ . Therefore equation 3.11 reduces to equation 3.12. This assumption is valid based on previous studies documented in literature (Zhang X. *et al.*, 2012).

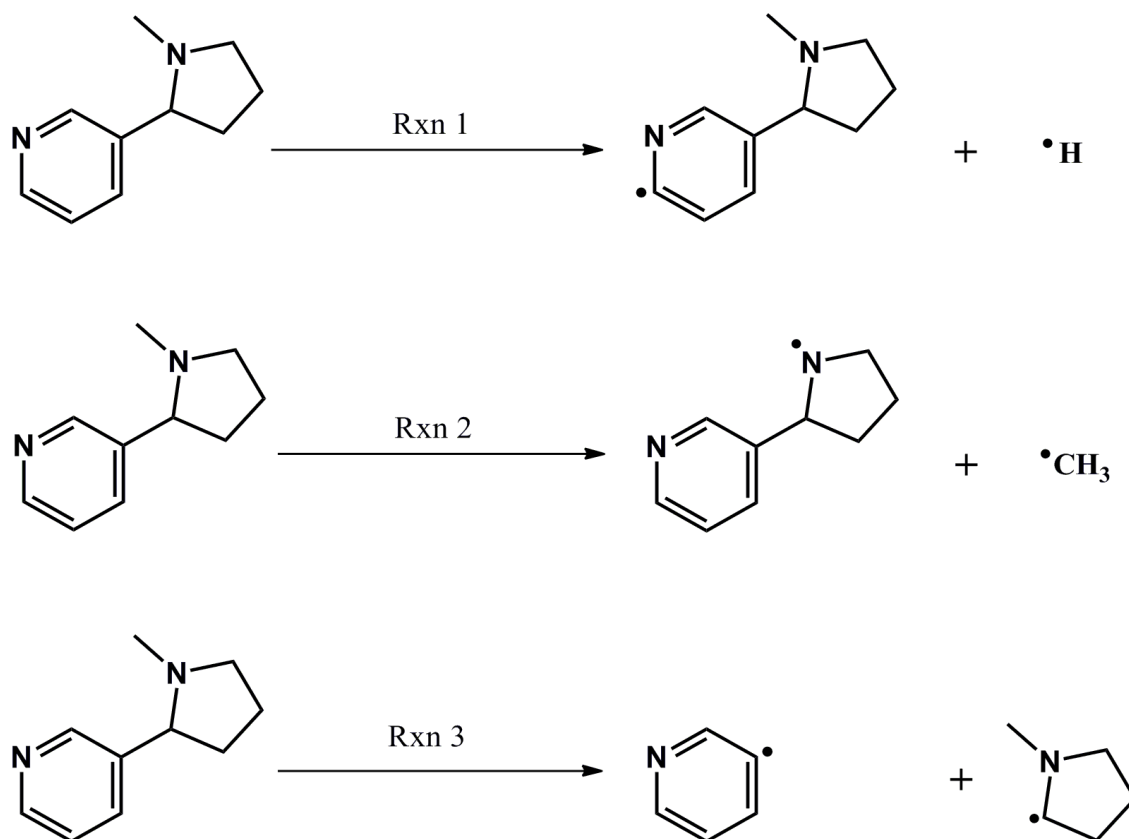
$$[\text{Product}] = [\text{Nic}]_0 \left( 1 - e^{-k_2 t} \right) \quad 3.12$$

## CHAPTER FOUR

### RESULTS AND DISCUSSION

#### 4.1 Choice of basis set used in computational calculations

In order to investigate the molecular behaviour and energetics of alkaloids identified in this work, thermochemical calculations were conducted using Gaussian '09 (Frisch *et al.*, 2009) computational framework for the purposes of quality assurance as well quality control. Nicotine was used as the test compound for selecting a suitable basis set (cf. scheme 4.1 and Figure 4.1). The geometries were optimized at DFT/B3LYP using the 6-31G basis set (Zhang Z. *et al.*, 2012). When using DFT, however; the choice of basis set is considered to be inconsequential because the convergence of DFT to the basis-set limit with increasing size of basis set is relatively quick, and as such, small basis sets are used. More often, diffuse functions on basis sets are not used for DFT calculations, as these lead to linear dependencies and a bad convergence of the self-consistent-field (SCF) Kohn–Sham equations for larger molecules (Boese, 2015).



**Scheme 4.1:** The formation of various radicals from the thermal degradation of nicotine

Quantum mechanical calculations are fundamental in predicting new insights on feasible mechanisms on the thermal degradation of environmental pollutants. Figure 4.1 shows the use of various basis sets for formation of different radicals from the thermal degradation of nicotine. It is evident that there are some slight differences between various basis sets though not significant. The most consistent basis set chosen for this investigation is the 6-31G which appears suitable for the tobacco alkaloids under investigation. Scheme 4.1, *vide supra* depicts the formation of various radicals in the proposed thermal degradation of nicotine in high temperature cigarette smoking. Clearly, reaction 2 proceeds with a lower energy in comparison to reactions 1 and 3. Accordingly, reaction 3 will form of a detailed mechanistic discussion in this study.

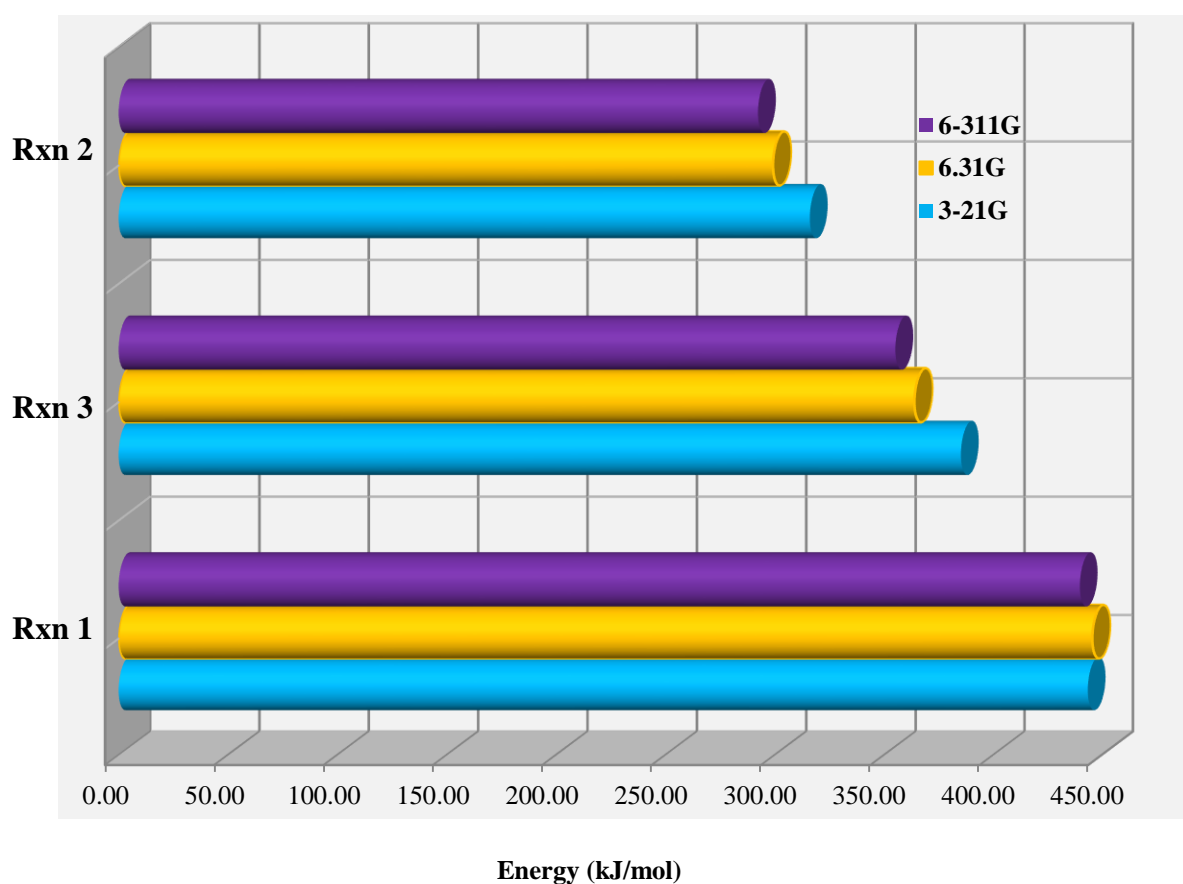


**Figure 4.1:** A plot of enthalpy change for reactions 1-3 (scheme 4.1) at various basis sets

#### 4.2 GC-MS characterization of selected alkaloids

In this study, it was established that the alkaloid content varied widely among the two commercial cigarettes investigated. The overlay chromatograms in Figure 4.2 indicate the characterization of the selected alkaloids reaction products explored in this work. The

compounds numbered *a* and *b* represent  $\beta$ -nicotyrine and 3, 5-dimethyl-1-phenylpyrazole respectively.

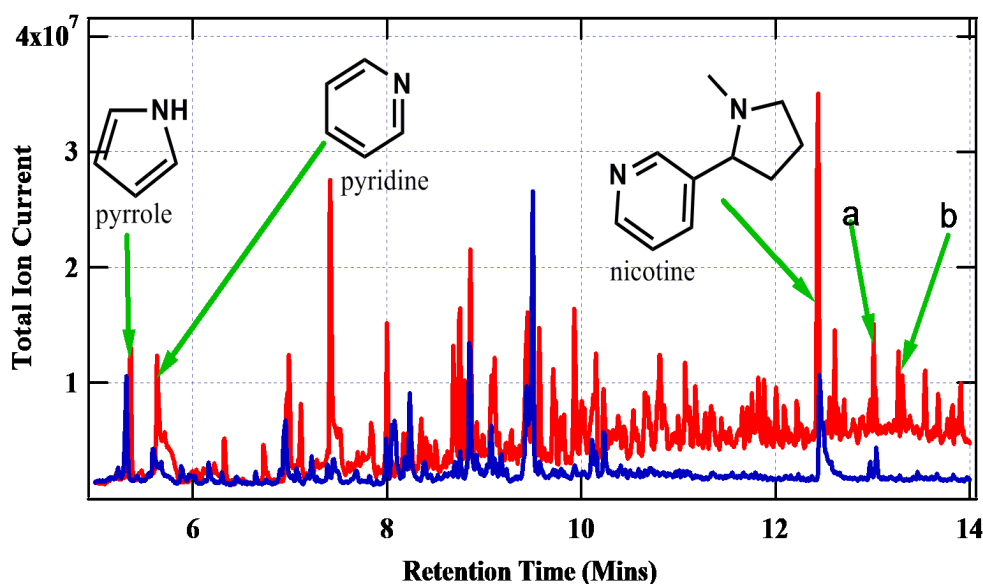


**Figure 4.2:** Overlay chromatograms for ES1 (red line) and SM1 (blue line) at 300 °C

#### 4.3 Product distribution of nicotine in ES1 and SM1 cigarettes

It is evidently clear that of all the alkaloids determined in this study, nicotine was found in high concentrations in the two commercial cigarettes in the entire pyrolysis temperature range as shown in Figure 4.3. The maximum concentration of nicotine was noted at 400 °C ( $\sim 8.0 \times 10^8$  GC-area counts) for ES1 cigarette, and peaked at  $\sim 520$  °C ( $\sim 2.7 \times 10^8$  GC-Area Counts) for SM1 cigarette. The variation in the maximum release temperature may be attributed to the composition of the cigarette during manufacturing processes. The ratio of total nicotine released by ES1 cigarette to that released by SM1 cigarette is  $\sim 10$ . This implies that ES1 cigarette contains nicotine by an order of magnitude than SM1 cigarette. These results are remarkable and present the first intense study on two different commercial cigarettes commonly sold in Kenya. The maxima of the two cigarettes give a ratio of  $\sim 3$ . This is a strong indication that ES1 has a high level of nicotine than SM1. Additionally, the evolution of nicotine from ES1 cigarette is significantly high even at low temperatures ( $\leq 300$  °C) as can be observed in Figure 4.3. On the contrary, nicotine production from SM1 cigarette only becomes significant above 300 °C.

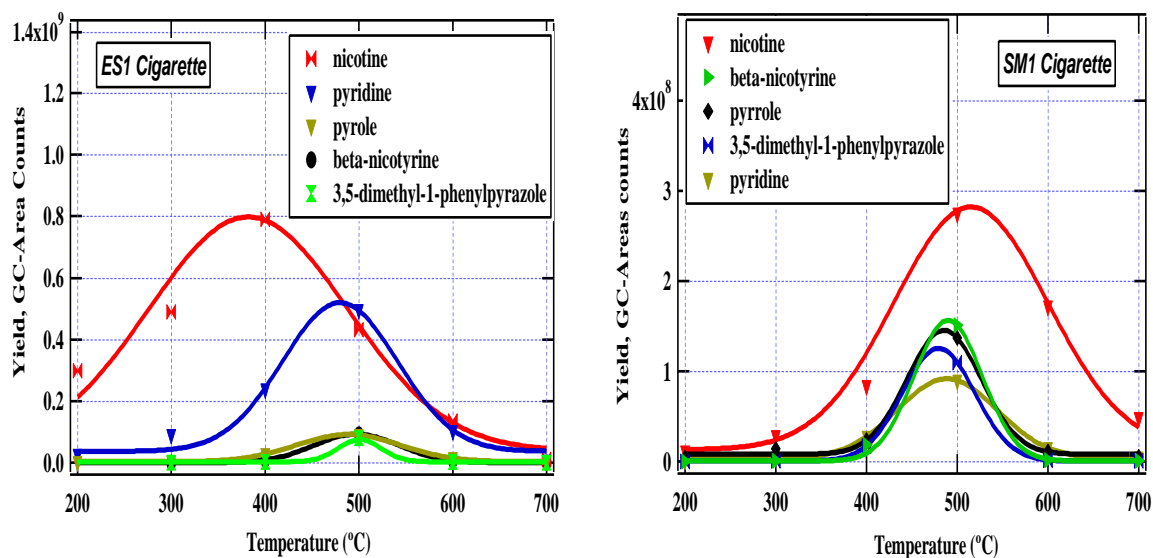


**Figure 4.3:** Product distribution of nicotine and the selected alkaloids in mainstream cigarette smoke determined from the burning of two commercial cigarettes; ES1 (left) and SM1 (right)

However, SM1 cigarette yields significantly high concentrations of  $\beta$ -nicotyrine and 3, 5-dimethyl-1-phenylpyrazole in the whole pyrolysis range in comparison to ES1 cigarette as shown in Figure 4.4. From these data alone, it can be noted that ES1 cigarette is very addictive considering the high levels of nicotine it produces during smoking.

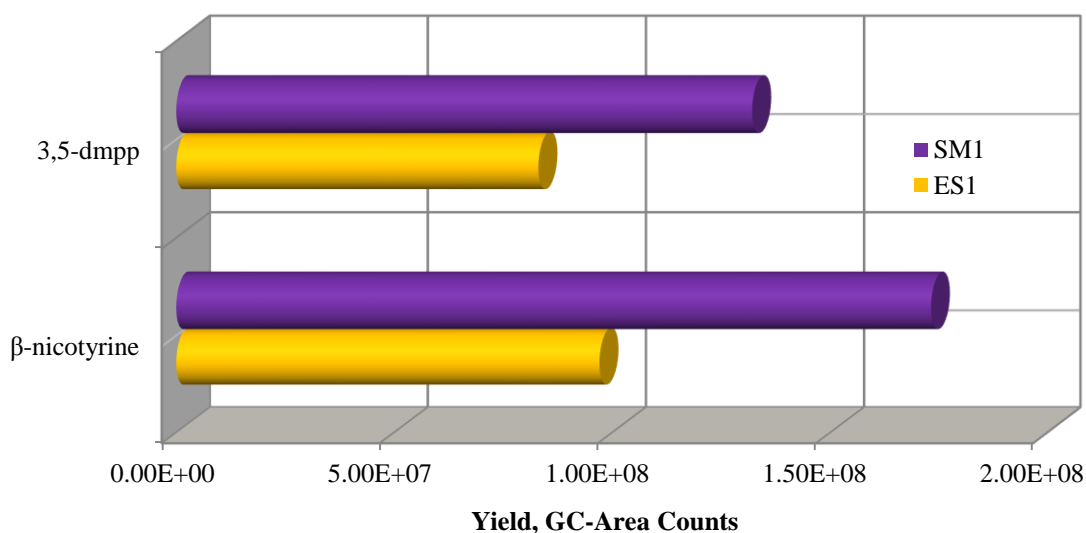


**Figure 4.4:** Product yields of  $\beta$ -nicotyrine and 3, 5-dimethyl-1-phenylpyrazole (3,5-dmpp) for ES1 cigarette (yellow) and SM1 (purple)

#### **4.4 Mechanistic pathways for radical formation and other possible molecular products**

The transformation of the selected tobacco alkaloids to their corresponding free radicals, intermediate by-products, and other possible alkaloids in tobacco has been explored using the density functional theory with the B3LYP hybrid correlation function in conjunction with the 6-31G basis set. Competing mechanistic pathways have been investigated and interesting data presented. The molecule in blue is the proposed starting alkaloid for the formation of various species indicated in the schematic reaction channels presented in this study. All computational calculations were conducted at a modest reaction temperature of 300 °C at 1 atmosphere. In all the schemes presented below, there are several parallel reaction pathways accompanied by different enthalpic barriers. For example in scheme 4.1, reactions 1 and 2 are the primary competing pathways for the thermal degradation of nicotine. Reactions 3 and 4, 5 and 6 are the other competing pathways for the transformation of intermediate radicals (pyridinyl and 1-methyl pyrrolidinyl respectively). Based on frequency analysis it was noted that all intermediates were at their minima and therefore all the structures presented in schemes 1-3 are fully optimized.

##### **4.4.1 Proposed mechanistic channel for the thermal degradation of nicotine**

This section investigates the possible mechanistic pathways involved during the thermal degradation of nicotine in tobacco burning to various intermediates and by-products. The loss of a methyl group (reaction 1) is accompanied by a less endothermic energy (302.13 kJ/mol) as compared to reaction 2 which proceeds with a modest endothermic energy of (365.33 kJ/mol). Whereas reaction 1 is expected to take place with minimum absorption of energy, it leads to the formation of few major intermediates; 3-(pyrrodin-2-yl) pyridinyl radical and possibly 3-(pyrrolidin-2-yl)pyridine. Thus these routes were not examined further considering the fact that 3-(pyrrolidin-2-yl) pyridine was not detected in mainstream cigarette smoke in the two cigarettes investigated. This leaves us to consider reaction 2 which results into many intermediates, some of which were detected experimentally in our studies. The scission of the phenyl-cyclopenta C-C linkage in nicotine resulting to the formation of pyridinyl and 1-methylpyrrolidinyl radical proves a very important pathway. Interestingly, reaction 3 and 5 are competing reaction channels for the formation of neutral species (3-methylpyridine and pyridine respectively). Since the hydride radical is more reactive than the methyl radical according to previous studies (Kibet *et al.*, 2012) then the formation of pyridine was expected to be produced in larger amounts than 3-methylpyridine. This observation was consistent

with the results obtained in this work. Accordingly, the product distribution of pyridine and 3-methylpyridine as a function of smoking temperatures has been presented in Figure 4.5 to validate the computational results explored in this study.

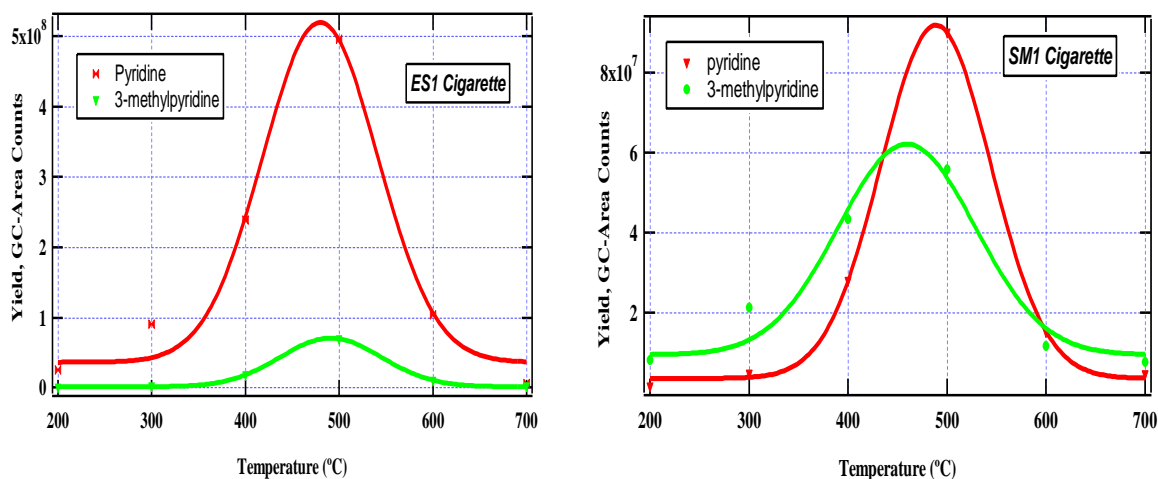
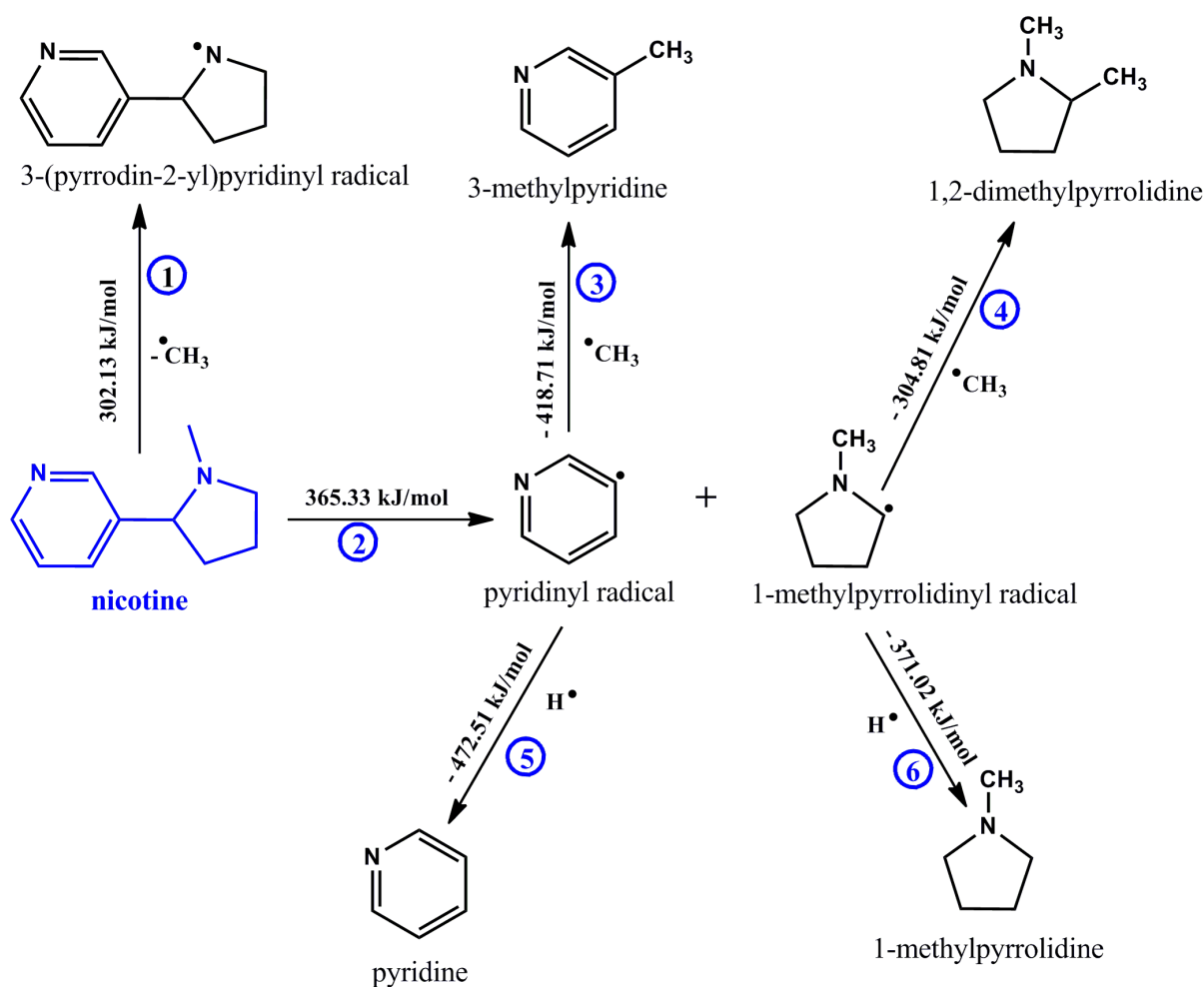


**Figure 4.5:** Product distribution of pyridine and 3-methylpyridine in mainstream cigarette smoke determined from the burning of commercial cigarettes; ES1 (**left**) and SM1 (**right**)

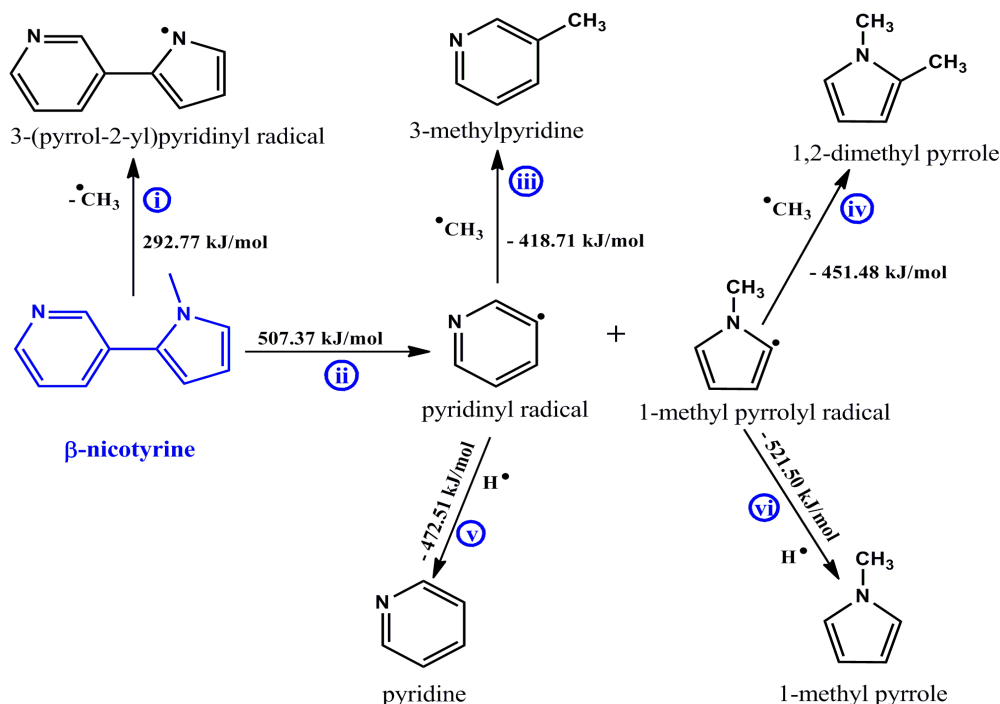
Pyridine, nevertheless was found to be high in ES1 cigarette and low in SM1 cigarette. On the other hand, reactions 4 and 6 are the other two parallel pathways. Although the formation of 1,2-dimethylpyrrolidine and 1-methylpyrrolidine were detected in low amounts in mainstream cigarette smoke for the two cigarettes under study, it is clear that reaction 6 proceeds with high exothermicity (-371.02 kJ/mol) and possibly more favourable than reaction 4 which proceeds with an enthalpic change of (-304.81 kJ/mol). The low exothermic value in reaction 4 may be attributed to the low reactivity of the methyl radical ( $\cdot CH_3$ ) in comparison to the reactivity of the hydride radical.



**Scheme 4.2:** Proposed mechanistic pathways for the thermal degradation of nicotine

#### 4.4.2 Mechanistic description for the thermal degradation of $\beta$ -nicotyrine

Although it may appear the molecular structure of  $\beta$ -nicotyrine and that of nicotine are similar, their chemistries are significantly different because of the influence of the  $\pi$ – $\pi$  in the C-C double bonds in the cyclopenta ring linkage which are absent in nicotine. These results in high bond dissociation energy for the phenyl/cyclopenta C-C bond presented by reaction *ii* (507.37 kJ/mol) compared to reaction 2 in scheme 4.2, *vide supra* and reaction *c*, scheme 4.4, *vide infra*. Another interesting reaction is reaction *i* which proceeds with an endothermicity of (292.77 kJ/mol) compared to reaction 1 which takes place with absorption of (302.13 kJ/mol scheme 4.2).



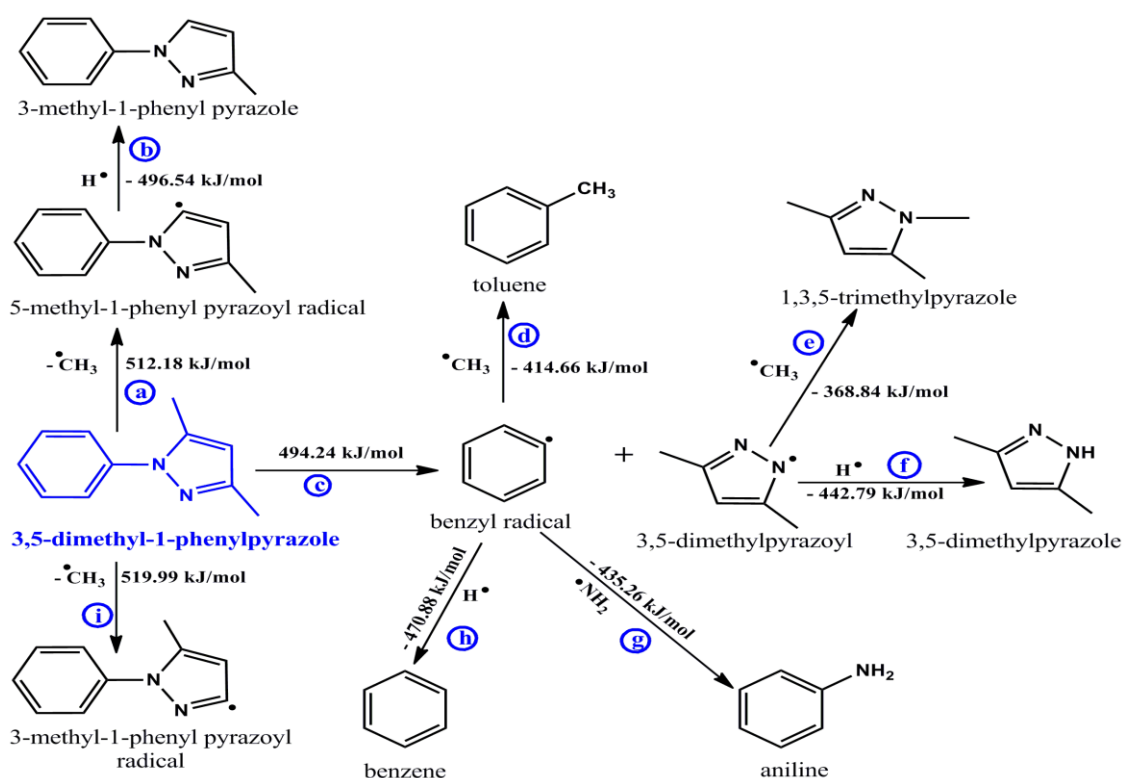
**Scheme 4.3:** Proposed mechanistic pathways for the thermal degradation of  $\beta$ -nicotyrine

The parallel reactions *iii* and *v* are very similar to reactions 3 and 5 in scheme 4.2. However, schemes 4.2 and 4.3 are responsible for the observed levels of pyridine and 3-methyl pyridine in cigarette smoke presented in Figs. 4.3 and 4.5. The formation of methylated pyrroles from 1-methylpyrrolyl radical is presented by the parallel reactions *iv* and *vi*. As previously discussed, the H radical is very reactive compared to the  $\text{CH}_3$  radical and therefore, 1-methylpyrrole will be expected to be formed in significant amounts in tobacco smoke. This result agrees well with our experimental results in which 1-methylpyrrole, though a minor product was detected in significant amounts as compared to 1, 2-dimethylpyrrole.

#### 4.4.3 The proposed mechanistic pathway for the thermal degradation of 3, 5-dimethyl-1-phenylpyrazole

The chemistry of 3, 5-dimethyl-1-phenylpyrazole is quite remarkable because its decomposition during cigarette smoking is predicted to yield several intermediate as well as stable by-products. The most important reaction products which were detected in significant amounts experimentally were toluene, benzene, and aniline which have successfully been predicted computationally in this scheme. Despite the fact that toluene and benzene are not the focus of this study, their products yields are presented in Figure 4.6 to qualify the theoretical explanations offered in scheme 4.4. Whereas the molecular structures of nicotine and  $\beta$ -nicotyrine contain a nitrogen atom in the phenyl ring, 3,5-dimethyl-1-phenylpyrazole

does not contain a nitrogen atom in the phenyl ring. This explains why 3,5-dimethyl-1-phenylpyrazole can easily form aromatic hydrocarbons (benzene and toluene) while nicotine and  $\beta$ -nicotyrine do not. Nevertheless, the bond dissociation energy for the phenyl C-N linkage in nicotine (302.13 kJ/mol, reaction 1) is much lower than in 3,5-dimethyl-1-phenylpyrazole (512.18 kJ/mol, reaction *a*) according to schemes 4.2 and 4.4 respectively. The ratio between the two energies is  $\sim 1.7$  indicating that the  $\pi - \pi$  interactions in the C-C double bonds and the phenyl nitrogen bond have a significant influence on the C-N bond in 3,5-dimethyl-1-phenylpyrazole. These groups are electron donating and therefore stabilize the methyl attached to the cyclopenta linkage in 3,5-dimethyl-1-phenylpyrazole. This makes it difficult for the  $\cdot CH_3$  to leave during the pyrolysis of tobacco. The scission of the methyl group in reaction *i* (scheme 4.4) occurs with higher endothermicity (519.99 kJ/mol). This again is attributed to the electron rich C-C double bond and the C-N bonds adjacent to the methyl which are electron donating and thus the methyl is strongly stabilized. The transformation of benzyl radical to molecular products (toluene, benzene, aniline) proceeds via three parallel pathways: reaction *d* (-414.66 kJ/mol), reaction *h* (-470.88 kJ/mol), and reaction *g* (-435.26 kJ/mol).



**Scheme 4.4:** Proposed mechanistic pathways for the thermal degradation of 3,5-dimethyl-1-phenylpyrazole

The formation of benzene from benzyl radical (reaction *h*) is the most preferred pathway because the hydride radical is more reactive than both the amine radical (reaction *g*) as well as the methyl radical (reaction *d*). Nonetheless, the amount of toluene formed from the combustion of the SM1 cigarette was found to be more than that of benzene implying that there might be other pyrosynthetic pathways in tobacco that result in the formation of toluene. Such possible pathways are beyond the scope of this investigation. Curiously, the amount of toluene and benzene for the ES1 cigarette were found to be similar according to Figure 4.6. To qualify the mechanistic description for the formation of benzene and toluene, product evolution curves of these compounds are presented in Figure 4.6 *vide infra*. Similar explanations can be inferred for the competing reactions *e* and *f*. Although methylated pyrazoles were detected in low amounts in our experiments, it is evident that the addition of H radical to the intermediate 3,5-dimethylpyrazoyl radical is the most favoured mechanistic channel because of the high exothermicity of (-442.79 kJ/mol).

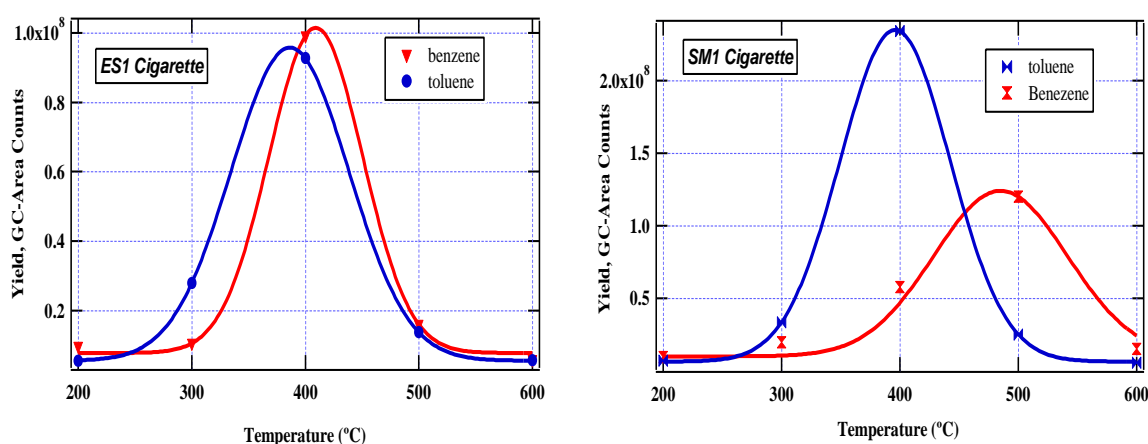


**Figure 4.6:** Product distribution of toluene and benzene in mainstream cigarette smoke determined from the burning of commercial cigarettes; ES1 (left) and SM1 (right)

While toluene and benzene reach a maximum at about the same temperature (~ 400 °C) for ES1 cigarette, the evolution characteristics of toluene and benzene for SM1 cigarette vary markedly. For instance, toluene peaks at 400 °C while benzene peaks at about 500 °C. Nevertheless, since toluene and benzene are not the principal attention of this work, their molecular behaviour as well as their toxicities will not be discussed further. However, one thing is certain; additives introduced to tobacco during processing and different growing conditions may affect the evolution characteristics of a reaction product.

## 4.5 Computational modeling of the selected alkaloids

### 4.5.1 Molecular geometries of major alkaloids

Geometrical parameters such as bond lengths and bond angles have a great influence on the strength of the bonds of molecular structures. Computational chemistry provides understanding into the molecular properties of a compound that would not be easy to determine experimentally. The optimization process presented *vide infra* shows steps towards achieving an optimized structure for nicotine,  $\beta$ -nicotyrine and 3, 5-dimethyl-1-phenylpyrazole. This is a fascinating quantum mechanics result that cannot easily be accomplished by experimental methods.

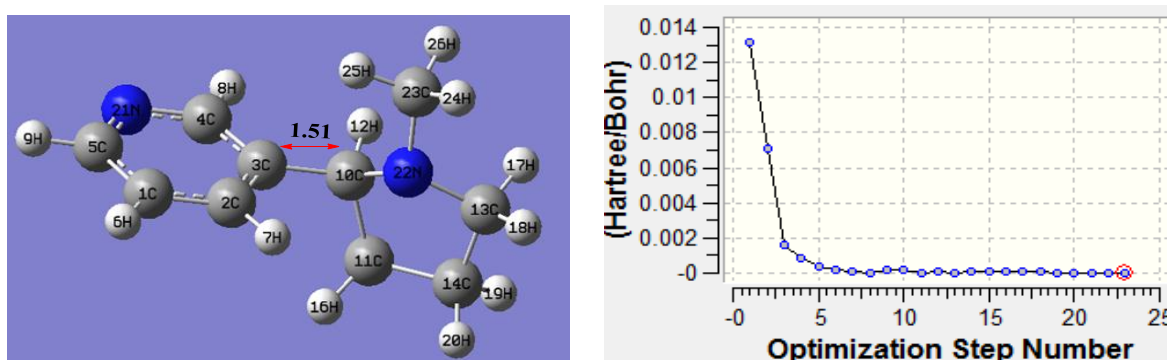


**Figure 4.7:** Optimized structure of nicotine and a plot showing its optimization steps (the red circle is the optimization level)

The scission of C3, C10 (1.51 Å) bond in nicotine proceeds with an energy of 365.33 kJ/mol and it required 23 steps to attain a structure of minimum energy usually referred to as the global energy.

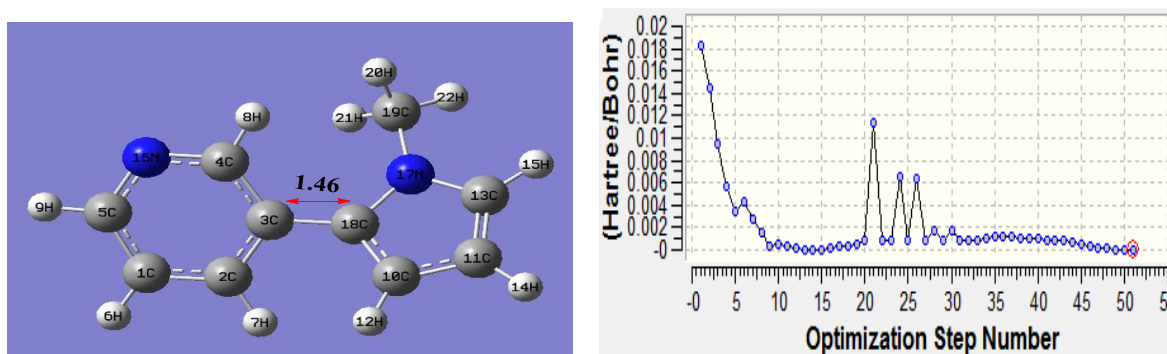


**Figure 4.8:** Optimized structure of  $\beta$ -nicotyrine and a plot showing its optimization steps (the red circle is the optimization level)

On the other hand  $\beta$ -nicotyrine required 52 steps to attain a structure of minimum energy while the breaking of C3, C18 (1.46 Å) bond takes place with a bond dissociation energy of 507.37 kJ/mol.

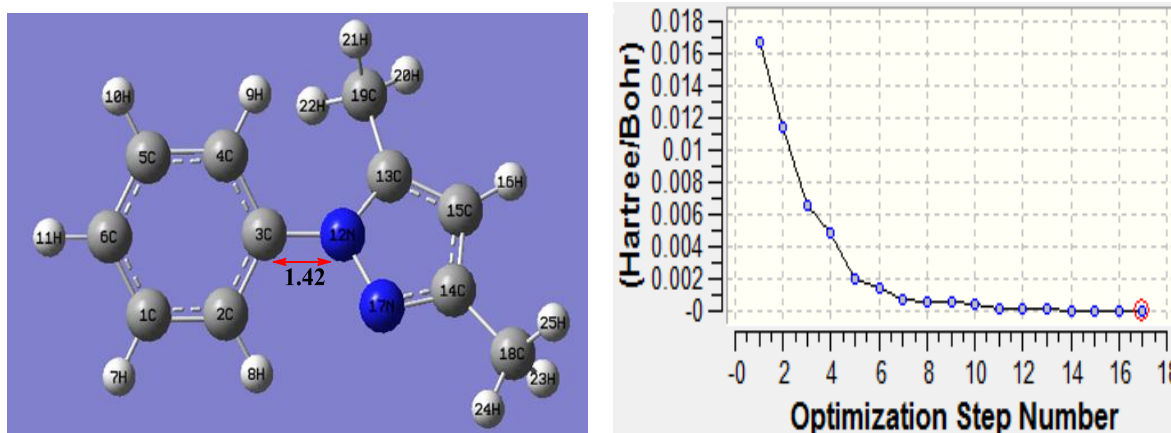


**Figure 4.9:** Optimized structure of 3,5-dimethyl-1-phenylpyrazole a plot showing its optimization step (the red circle is the optimization level)

3,5-dimethyl-1-phenylpyrazole required only 17 steps to attain a structure of minimum energy while the scission of C3, N12 (1.42 Å) bond in 3,5-dimethyl-1-phenylpyrazole occurs with a bond dissociation energy of 494.24 kJ/mol.

The bond strength increases from nicotine to  $\beta$ -nicotyrine to 3,5-dimethyl-1-phenylpyrazole as presented in Figure 4.7 – 4.9. This implies that, the shorter the bond length, the higher the bond dissociation energy. This is consistent with the thermochemical results presented in schemes 4.2, 4.3 and 4.4. The phenyl bond dissociation in  $\beta$ -nicotyrine and 3,5-dimethyl-1-phenylpyrazole are effectively stabilized by the  $\pi - \pi$  interactions than in nicotine molecule.

#### 4.5.2 Molecular orbitals and electron density maps of nicotine

The HOMO and the LUMO are conventional acronyms for the highest occupied and lowest unoccupied molecular orbitals respectively. These orbitals are the pair that lie nearest in energy of any pair of orbitals in any two molecules, which permits them to interact more strongly (Frisch *et al.*, 2009). The HOMO-LUMO band-gap energies for the alkaloids under study are presented in Table 4.1. The reactivity index (band gap) of the compounds with small difference implies high reactivity and a large difference implies low reactivity in reactions, therefore as the energy gap between the HOMO and LUMO becomes smaller the rate of reaction is favoured.  $\beta$ -nicotyrine has the smallest HOMO-LUMO energy gap (4.811

eV) and therefore more reactive compared to nicotine (5.492 eV) and 3, 5-dimethyl-1-phenylpyrazole (6.057 eV). Though 3,5-dimethyl-1-phenylpyrazole may have a large HOMO-LUMO energy gap it is considered a good electron donor (Hanulikova *et al.*, 2016).

**Table 4.1:** HOMO-LUMO band gap energies for the selected alkaloids under study

<i>Compound</i>	$E_{HOMO} (eV)$	$E_{LUMO} (eV)$	$\Delta E = E_{LUMO} - E_{HOMO} (eV)$
Nicotine	-5.974	-0.482	5.492
$\beta$ -nicotyrine	-5.837	-1.026	4.811
3,5-dimethyl-1-phenylpyrazole	-6.213	-0.156	6.057

In this investigation, the HOMO-LUMO band-gap of nicotine and  $\beta$ -nicotyrine are significantly low and may be reactive especially towards biological structures. This may explain the fact that nicotine is immediately adsorbed into the blood stream and reaches the brain in 10–20 s seconds after a cigarette puff as reported in literature (Benowitz *et al.*, 2009). Generally, the band-gap between the HOMO and the LUMO is directly related to the electronic stability of the chemical species (Hanulikova *et al.*, 2016). This suggests that 3, 5-dimethyl-1-phenylpyrazole having a lower HOMO energy value of -6.213 eV is much more stable making it a good nucleophile compared to nicotine and  $\beta$ -nicotyrine which are energetically higher in the HOMO; -5.974 eV and -5.837 eV respectively.

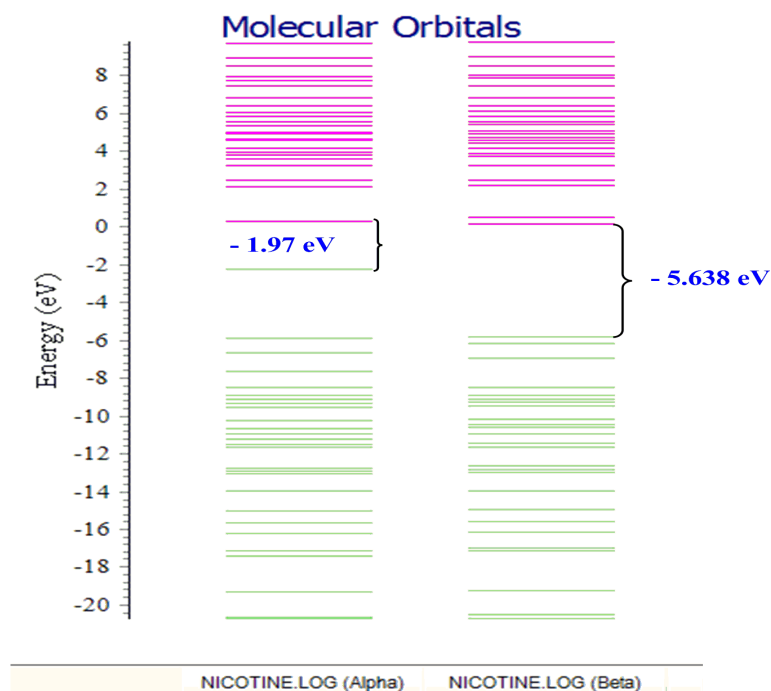


**Figure 4.10:** The HOMO-LUMO band gap for nicotine determined using Chemissian

Computational calculations therefore predict areas where interactions can occur to cause a reaction. They give possible reaction mechanisms which the molecules can undergo. Despite continuing improvements in formulating new DFT functionals with advanced predictive capabilities, the B3LYP functional retains its comparative accuracy in general applications to organic systems (Uddin *et al.*, 2012; Boese, 2015). The application of Chemissian software facilitated the construction of electron density contour maps and molecular orbitals from which the band gap between the HOMO and the LUMO of nicotine,  $\beta$ -nicotyrine and 3, 5-dimethyl-1-phenylpyrazole were calculated.

The electron density contours maps for 2D-, 3D-, and 1-dimensions for nicotine are presented in Figures 4.11 – 4.13 respectively. Electron density maps are very important in understanding electrophilic and nucleophilic sites. Conventionally, the negative potential sites (red colour) represents regions of electrophilic reactivity and interactions through  $\pi$ - $\pi$  bonding within aromatic systems and positive potential sites (blue colour) represents regions of nucleophilic reactivity (Hanulikova *et al.*, 2016). Similar electron density maps were done for  $\beta$ -nicotyrine and dimethyl-1-phenylpyrazole as presented in appendix 1 and 2. These figures are critical in determining regions of high electron density within a molecule. Electron

distribution gives insight on the behaviour of a particular toxicant and probably the binding site during reactions with biological molecules such as DNA, microsomes, and lipids.

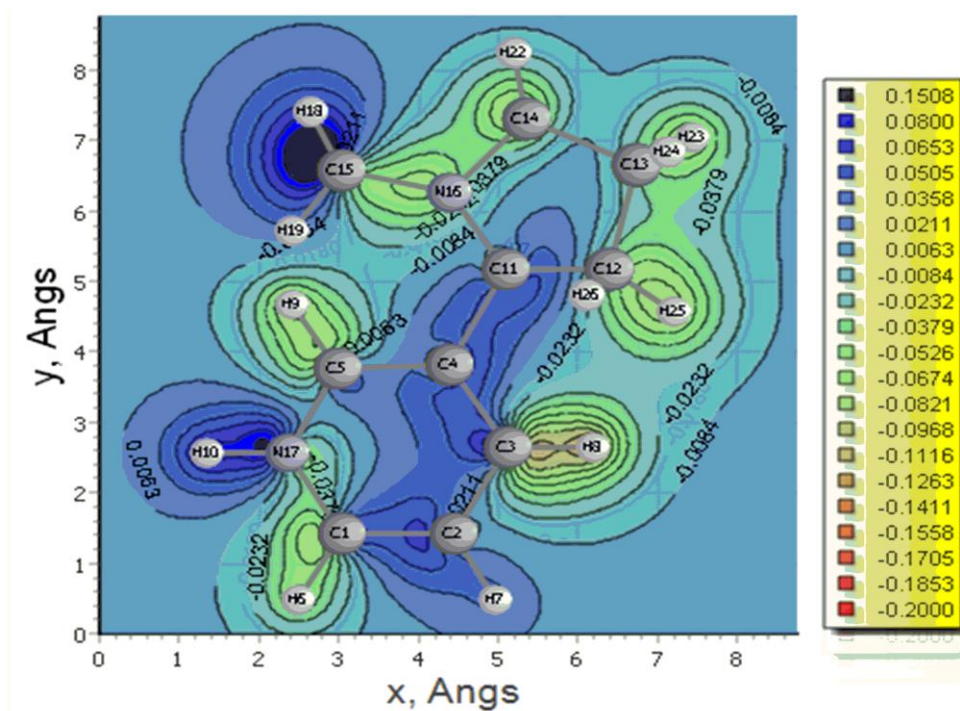


**Figure 4.11:** 2-D electron density map for nicotine

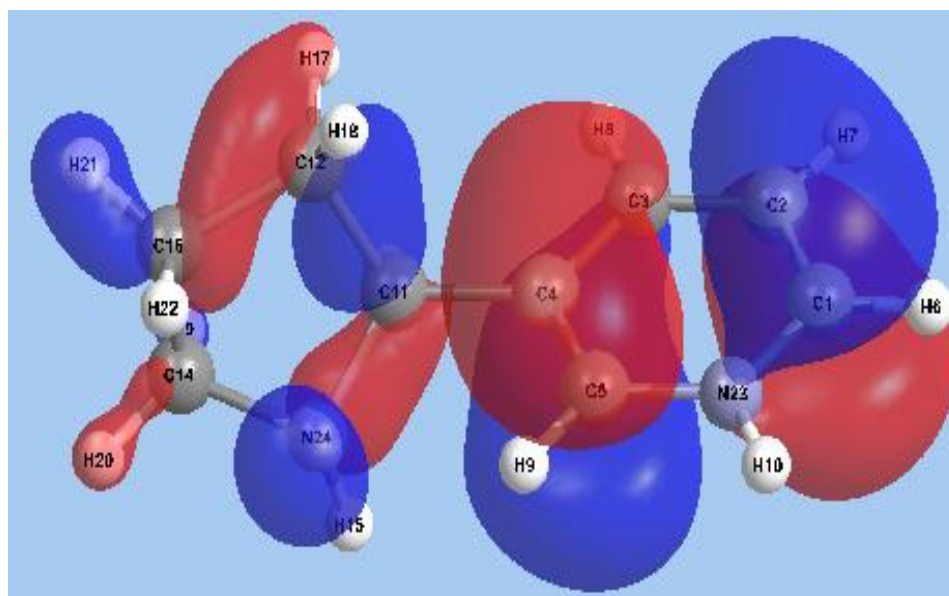


**Figure 4.12:** 3-D molecular orbital diagram showing electronic density for nicotine at an isovalue of 0.02

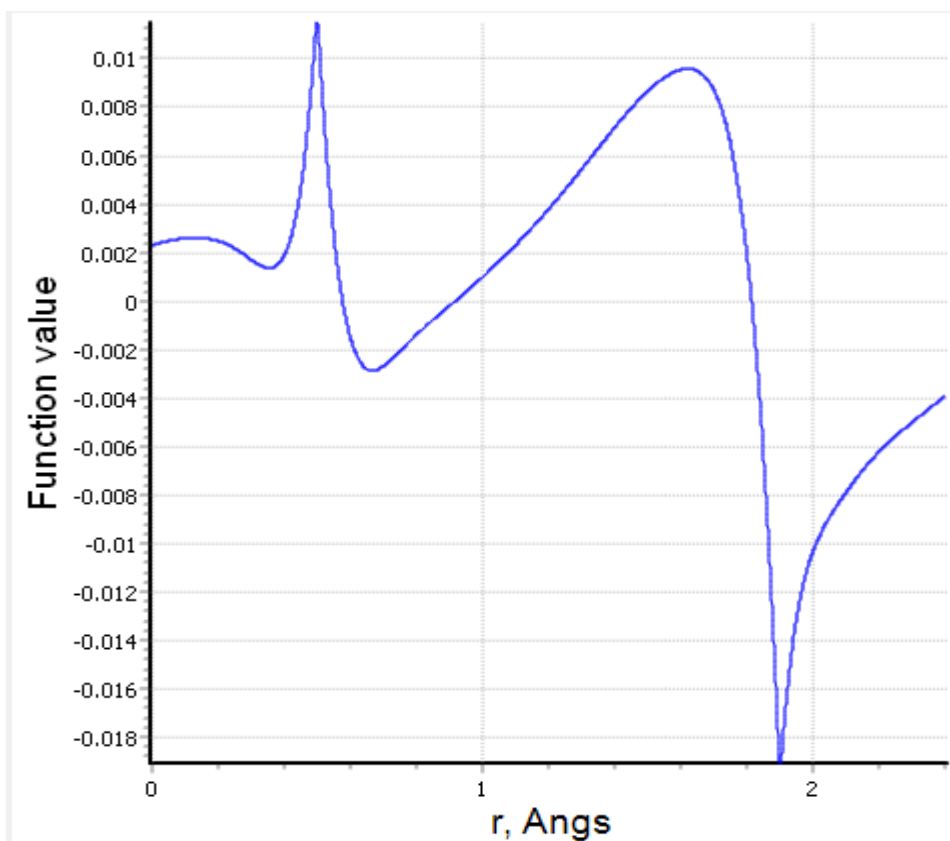


**Figure 4.13:** 1-D line showing the probability of finding electrons at a distance  $r$  from nicotine nuclei

#### 4.6 Decomposition profile of tobacco

The decomposition characteristics of tobacco over the temperature range of 200 -700 °C gave interesting results as shown in Figure 4.14. The initial sharp decrease in % char to ~ 80% at 200 °C may be attributed to high mass loss of water and other volatiles in the tobacco sample. Significant mass loss was also registered between 200 °C and 400 °C (~ 30% mass loss). This was consistent with other results of biomass pyrolysis which indicate the higher mass loss of biomass pyrolysis occurs in this temperature region (Sharma and Hajaligol, 2003). The mass loss between 400 and 500 °C was ~17%. This region coincides with the highest release of molecular toxins. Thus, by 500 °C most organic compounds will have been formed so that any further increase in temperature results in sharp decrease in the pyrolysis products (Fig. 4.3). These results corroborate previous data reported in literature on biomass pyrolysis (Kibet *et al.*, 2014).

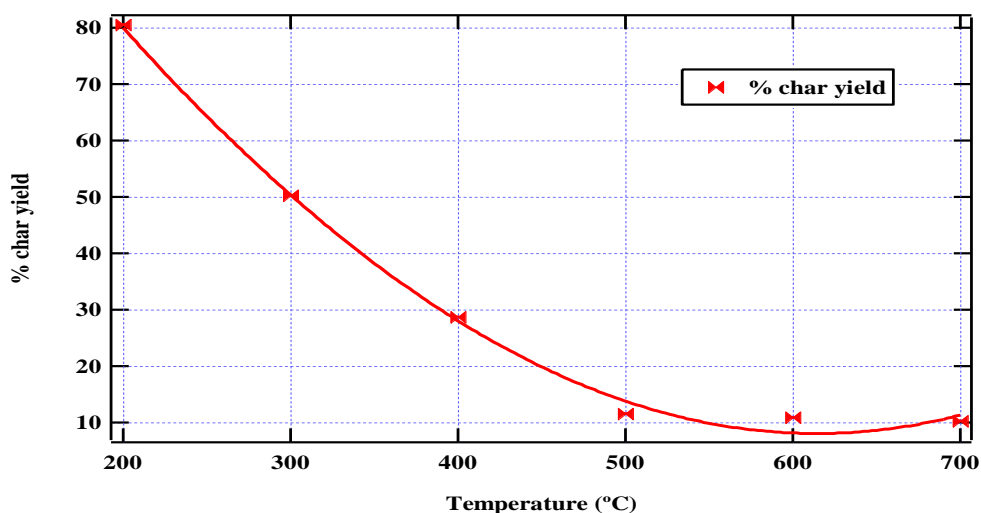


**Figure 4.14:** Percentage (%) yield of char from tobacco

The lowest mass was recorded at 700 °C (~10%). The mass loss was fairly constant between 600 °C and 700 °C.

#### 4.7 The formation and destruction kinetics of nicotine

To mimic actual cigarette smoking conditions, smoking apparatus were designed according to ISO 3402:1999 standards. Whereas the destruction kinetics of nicotine was explored for both ES1 and SM1 cigarettes, only ES1 cigarette was investigated for nicotine formation. For formation kinetics, smoking residence times usually representative of real world cigarette smoking conditions (2, 5, and 10 seconds) were explored. Consequently, a plot of  $\ln C$  as a function of puff (smoking) time yielded a straight line with a slope of  $-0.1323$  (Figure 4.15) from which the formation rate constant of nicotine ( $0.13s^{-1}$ ) was calculated. The plot, although an estimation from restricted smoking times is consistent with first order reaction kinetics. The original amount of nicotine in ES1 cigarette was estimated from the y-intercept and established to be  $9.1 \times 10^8$  GC-Area counts. This value is remarkably close to that obtained from experimental modeling  $\sim 8.0 \times 10^8$  GC-Area counts.

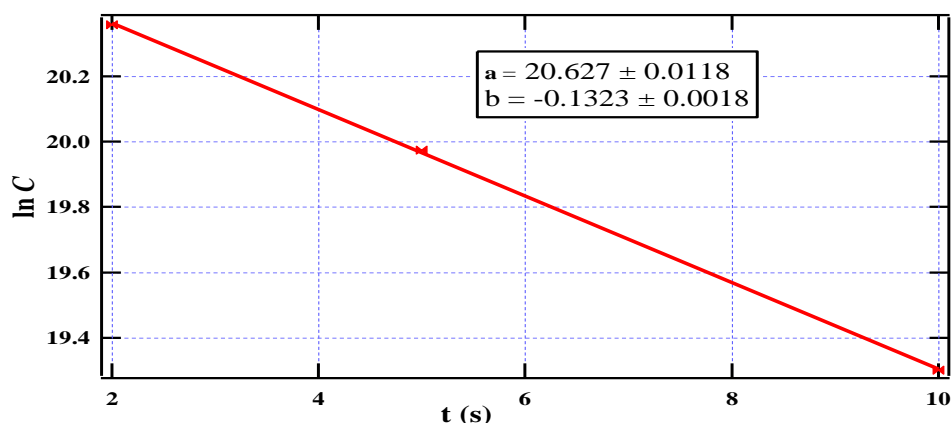


**Figure 4.15:** Formation kinetics of nicotine

The destruction kinetics revealed that nicotine from ES1 cigarette proceeds with activation energy of 108.85 kJ/mol while SM1 takes place with activation energy of 136.52 kJ/mol as presented in Table 4.2. These results are comparable to the results reported in literature in which the average activation energy of nicotine was found to be 120 kJ/mol (Forster *et al.*, 2015) This implies that the two cigarettes may have different matrix composition. Thus the activation energies of nicotine in the two cigarettes may not necessarily be the same considering the fact that additives of varying composition introduced during cigarettes processing may act as catalysts and ultimately reduce the activation energy of a given compound in a complex biomass material such as tobacco.

**Table 4.2:** The Arrhenius parameters for the destruction of nicotine from the pyrolysis of two commercial cigarettes (ES1 and SM1)

Cigarette Type	$E_a$ (kJ / mol)	$A$ ( $s^{-1}$ )
ES1	108.85	$2.1 \times 10^6$
SM1	136.52	$3.0 \times 10^7$

Arrhenius plots for the destruction of nicotine from the cigarettes under study are presented in Figure 4.16, *vide infra*. The activation energies obtained from this work are comparable with results from the kinetic modelling of other biomass pyrolysis such as cellulose(Zhang Z. *et al.*, 2012).

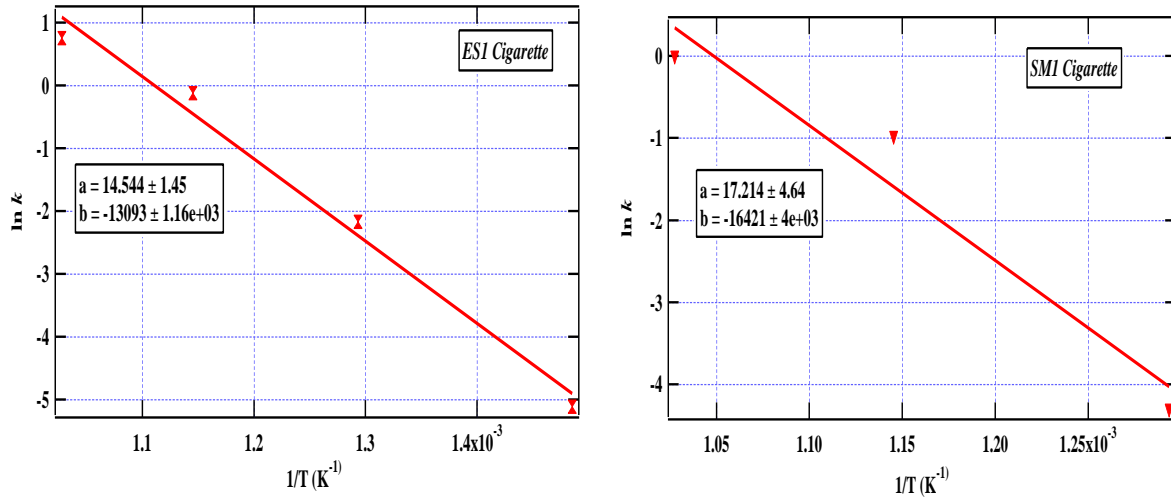


**Figure 4.16:** Arrhenius plots for the destruction kinetics of nicotine in ES1 and SM1 cigarettes

Nonetheless, in modelling the destruction kinetics of nicotine, it is known that kinetic characteristics of a given heterogeneous system such as plant matter may change during the process of pyrolysis and so it is possible that the complete reaction mechanism cannot be represented adequately by a specific kinetic model (White *et al.*, 2011; Wang *et al.*, 2012).

The destruction rate constant  $k_1$  at 673 K for ES1 was  $0.31\text{s}^{-1}$  while that of SM1 at the same temperature was estimated as  $0.74\text{s}^{-1}$ . At the highest pyrolysis temperature (973 K), the respective rate constants were  $2.12\text{s}^{-1}$  and  $1.0\text{s}^{-1}$  respectively.

In order to estimate the Arrhenius dependent rate constants consistent with experimental rate constants the modified Arrhenius rate law was applied (Equation 4.1).

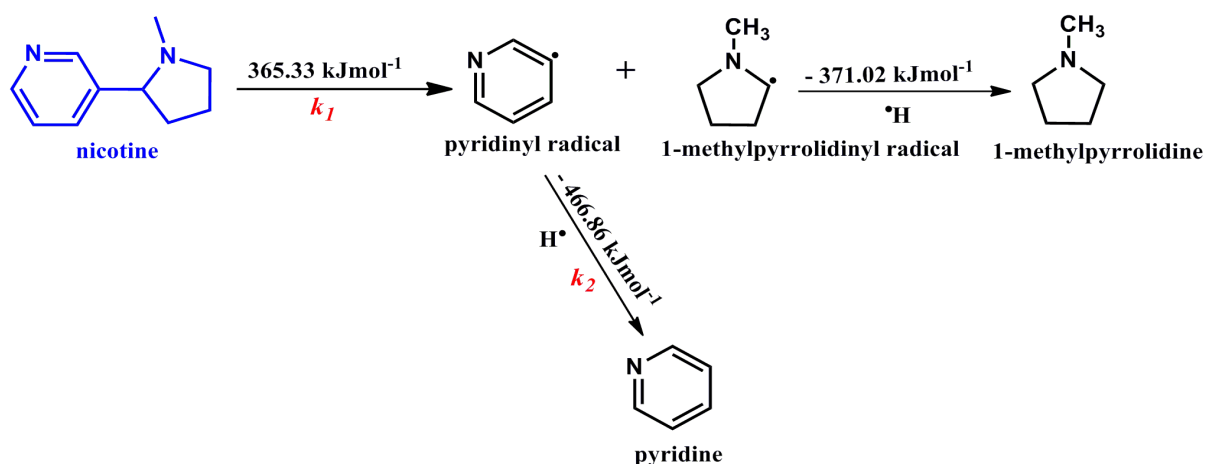
$$k = AT^n e^{-\frac{Ea}{RT}} \quad 4.1$$

Since the rate constant for a given temperature was determined experimentally and all the other parameters had been calculated, the value of n was determined from equation 4.1. For instance, the value of n at 673 K was determined and found to be 0.55 and 1.05 for the destruction of nicotine in ES1 and SM1 cigarettes respectively. Equation 4.1 can be used to estimate the value of n at any particular temperature since the rate constants are temperature dependent.

Accordingly, the average destruction rate constant for ES1 ( $1.11 \text{ s}^{-1}$ ) was about 1 magnitude the formation rate constant presented in Figure 4.15 ( $0.13 \text{ s}^{-1}$ ). This suggests that the rate of destruction is much higher than the rate of formation because the latter occurs at high temperatures. Table 4.2 presents the Arrhenius parameters from the destruction kinetics of nicotine (Activation energies and Arrhenius factors). Whereas the activation energies are comparably close, the pre-exponential factors for the two cigarettes under study differ by a whole magnitude.

#### 4.8 The proposed mechanistic pathways for the destruction of nicotine

The proposed mechanism for the formation of pyridine from nicotine is presented in scheme 4.5 *vide infra*. All the energies shown in the scheme were estimated quantum mechanically using the Density Functional Theory (DFT).



**Scheme 4.5:** Mechanistic destruction of nicotine to radical intermediates and possible by-products

From scheme 4.5 above the bond dissociation energy via  $k_1$  and the bond formation energy via  $k_2$  were estimated using the density function theory framework at the B3LYP energy functional in conjunction with 6-31G basis set, hence the scheme proposes a mechanistic pathway for the thermal degradation of nicotine to the intermediate (pyridinyl radical) and eventually pyridine.

#### 4.9 Toxicological implications of molecular products from cigarette smoke

Several scientific and epidemiological evidences have explicitly established that cigarette smoking is a risk factor for various degenerative diseases such as cancer of the lungs and

other organs and cardiovascular disease. Even in smokers without any obvious clinical symptoms, the overall life expectancy is reduced, ranging up to 10 years fewer than non-smokers (Ghosh *et al.*, 2012). The radicals generated during cigarette smoking are generally hazardous as they have the possibility of reacting with biological tissues such as DNA, lipids and lung macrophages to initiate tumours, cancer and oxidative stress. In this study, the radicals including pyridinyl, benzyl, 1-methyl pyrrolyl, and 1-methylpyrrolidinyl radicals are good candidates for cell injury and oxidative stress during cigarette smoking. It is well known in literature that approximately  $10^{16}$  alkyl- and alkoxy radicals are present in the gas-phase of one cigarette, or  $5 \times 10^{14}$  radicals per puff (Borgerding and Klus, 2005). These types of radicals are not only short-lived but also responsible for serious biological damage to the health of cigarette smokers. Nevertheless, some studies have shown that cigarette smoke radicals may have longer lifetimes of up to 5 min although the exact nature of these radicals is yet to be understood. The toxicity of a cigarette smoke is believed to be a function of the concentrations of individual toxicants present in smoke (Blakley *et al.*, 2001). Molecular products of tobacco including alkaloids are metabolized, primarily in the liver, to a series of ring-opened products which cause severe alveoli and other cell injuries. This makes alkaloid-based radicals such as those presented in schemes 4.2-4.4, *vide supra* potential clinical candidates for a myriad of ailments affecting smokers. These include aging, cancer, stroke, and cardiopulmonary death.

There is no doubt that inhaled toxicants such as alkaloids in cigarette smoke can cause both irreversible alterations to the DNA and serious variations in the genetic landscape which include changes in the DNA methylation and chromatin alteration state. Clearly, from this study, alkaloids and their corresponding free radicals are potential candidates for diseases that are believed to comprise genetic and epigenetic perturbations such as lung cancer, chronic obstructive pulmonary disease (COPD), and cardiovascular disease (CVD), all of which are strongly associated epidemiologically to cigarette smoking. Lung cancer development includes various genomic aberrations, such as point mutations, deleterious effects, and gene enlargements (Talikka *et al.*, 2012). Additionally, reproductive function and fertility are believed to be compromised by behaviors such as cigarette smoking (Sadeu *et al.*, 2010). Although very little information is available in literature on the effects of  $\beta$ -nicotyrine and 3,5-dimethylpyrazole, it is evident from this study that their molecular nature as well as their intermediate radicals may pose critical impacts to the biological structures of cigarette

smokers. The molecular structure of nicotine and other alkaloid related compounds investigated in this work may covalently bond to the DNA, lipids, nuclei acids, and body cells before metabolizing into harmful by-products that are potential risks to the human health (Dellinger *et al.*, 2000; Bolton *et al.*, 2000; Elshal *et al.*, 2009).

## CHAPTER FIVE

### CONCLUSION AND RECOMMENDATIONS

#### 5.1 Conclusion

This study has presented a thorough mechanistic description on the molecular characteristics of major alkaloids (nicotine,  $\beta$ -nicotyrine, and 3, 5-dimethyl-1-phenylpyrazole) never presented before in literature. It was established that the concentration of nicotine in ES1 cigarette was  $\sim 10$  times the concentration of nicotine evolved in SM1 cigarette. Based on nicotine results alone, it is evident ES1 cigarette is more addictive than SM1 cigarette and consequently more toxic. The activation energy for nicotine obtained from this investigation is consistent with that obtained by other researchers as reported in literature.

The consistency between experimental formation of pyridine, 3-methylpyridine, toluene, and benzene, and computational predictions is remarkable. It was also established in this study that most of the alkaloids were evolved between 300 and 500 °C. Clearly, this is a region that should be avoided in the design of modern cigarettes since most organic toxics are released in high yields in this temperature range. Cigarettes that can be smoked at a lower temperature would therefore be beneficial. Nonetheless, for ES1 cigarette, low temperature cigarette smoking may not necessarily reduce the levels of nicotine uptake by smokers. It was also established that the strength of the C-C and C-N bonds in phenyl linkages in the alkaloids investigated in this study were dependent on the  $\pi - \pi$  interactions which stabilize the bonds. Therefore because of the small bond dissociation energy required to break the phenyl C-C linkage in nicotine (365.33 kJ/mol) compared to (507.37 kJ/mol) required to break the C-C phenyl bond in  $\beta$ -nicotyrine, it is apparent that most of the yields of pyridine and 3-methylpyridine observed from our experiments are proposed to originate from the thermal degradation of nicotine.

The temperature dependent destruction kinetics of nicotine has been presented for the first time in this investigation. We therefore believe these results will form the basis of further research towards understanding the addictive mechanism of nicotine in the human brain and the nervous system. The two cigarettes investigated in this work coded ES1 and SM1 have exhibited various kinetic characteristics possibly because of their different biomass composition attributed mainly to their growing conditions and additives during tobacco

processing. The concentration of the intermediate (pyridinyl radical) has been estimated from kinetic modeling of nicotine. This is remarkable since the concentrations of intermediates in complex reaction systems such as biomass are usually tedious to determine experimentally.

Therefore, in the development of modern cigarettes, emphasis should be towards developing cigarettes that can be smoked at optimum temperatures (below 300 °C) which do not favour the formation of high levels of nicotine. Nonetheless, it must be noted that nicotine cannot be eliminated completely even at low smoking temperatures and therefore the safest way is to quit cigarette smoking completely. This is not an easy task owing to the addictive nature of nicotine but efforts must be to sensitize the general public on the hazards of cigarette smoking.

## **5.2 Recommendations**

This work has thoroughly investigated the release of major tobacco alkaloids during cigarette smoking. The energetics and the kinetic behaviour of these alkaloids were also considered critically from a theoretical standpoint. Nonetheless, a lot of work needs to be done in order to exhaustively draw serious conclusions on the consumption of tobacco. The following are recommendations that can be drawn from this study.

1. Smoking temperatures of cigarettes should be regulated to avoid situations where high levels of toxic compounds are released. Therefore this study recommends designing cigarettes that can be smoked at optimum temperatures of  $\leq 300$  °C based on the results reported in this work.
2. The formation kinetics of other major pyrolysis products of tobacco such as pyridine, benzene and toluene should be explored in future studies.
3. There is need to monitor the growing conditions of tobacco, processing, and packaging to ensure minimal input of toxins from fertilizers and additives such as flavours during tobacco processing.
4. In order to clearly understand the interaction of tobacco alkaloids with biological tissues such as DNA and neuron transmitters, this study recommends molecular docking in order to investigate the binding sites of these alkaloids in biological structures.

## REFERENCES

- Abrams, D. B. and Niaura R. (2003). *The tobacco dependence treatment handbook: A guide to best practices*. Seventh Avenue Suite, New York, USA: Guilford Press.
- Adam, T., McAughey J., Mocker C., McGrath C. and Zimmermann R. (2010). Influence of filter ventilation on the chemical composition of cigarette mainstream smoke. *Analytica Chimica Acta*, **657**: 36-44.
- Anand, P., Kunnumakara A. B., Sundaram C., Harikumar K. B., Tharakan S. T., Lai O. S., Sung B. and Aggarwal B. B. (2008). Cancer is a preventable disease that requires major lifestyle changes. *Pharmaceutical Research*, **25**: 2097-2116.
- Anderson, J., Jorenby D., Scott W. and Fiore M. (2002). Treating tobacco use and dependence: an evidence-based clinical practice guideline for tobacco cessation. *Chest Journal*, **121**: 932-941.
- Armitage, A., Dollery C., Houseman T. , Kohner E., Lewis P. and Turner D. (1978). Absorption of nicotine from small cigars. *Clinical Pharmacology and Therapeutics*, **23**: 143-151.
- Armitage, A. K., Dixon M., Frost B. E., Mariner D. C. and Sinclair N. M. (2004). The effect of inhalation volume and breath-hold duration on the retention of nicotine and solanesol in the human respiratory tract and on subsequent plasma nicotine concentrations during cigarette smoking. *Contributions to Tobacco Research*, **21**: 240-249.
- Babu, B. V. (2008). Biomass pyrolysis: a state-of-the-art review. *Biofuels, Bioproducts and Biorefining*, **2**: 393-414.
- Baker, R. R. (2006). Smoke generation inside a burning cigarette: modifying combustion to develop cigarettes that may be less hazardous to health. *Progress in Energy and Combustion Science*, **32**: 373-385.
- Baker, R. R. (2007). Sugars, carbonyls and smoke. . *Food and Chemical Toxicology*, **45**: 1783-1786.

- Benowitz, N. (1988). Drug therapy. Pharmacologic aspects of cigarette smoking and nicotine addiction. *The New England Journal of Medicine*, **319**: 1318-1330.
- Benowitz, N. (1990). Clinical pharmacology of inhaled drugs of abuse: implications in understanding nicotine dependence. *NIDA Research Monograph Journal*, **99**: 12-29.
- Benowitz, N. (1996). Pharmacology of nicotine: addiction and therapeutics. *Annual Review of Pharmacology and Toxicology*, **36**: 597-613.
- Benowitz, N. (1999). Nicotine addiction. *Primary Care: Clinics in Office Practice*, **26**: 611-631.
- Benowitz, N. (2001). Trans-3'-hydroxycotinine: Disposition kinetics, effects and plasma levels during cigarette smoking. *British Pharmacological Society*, **51**: 53-59.
- Benowitz, N. (2008). Neurobiology of Nicotine Addiction: Implications for Smoking Cessation Treatment. *The American Journal of Medicine*, **121**: 3-10.
- Benowitz, N. (2010). Nicotine Addiction. *Pharmaceutical Research*, **362**: 2295-2303.
- Benowitz, N., Hukkanen J. and Jacob P. (2009). Nicotine Chemistry, Metabolism, Kinetics and Biomarkers. *Handbook of Experimental Pharmacology*, **192**: 29-60.
- Benowitz, N. and Jacob P. (1994). Metabolism of nicotine to cotinine studied by a dual stable isotope method. *Clinical Pharmacology and Therapeutics*, **56**: 483-493.
- Blakley, R., Henry D. and Smith C. (2001). Lack of correlation between cigarette mainstream smoke particulate phase radicals and hydroquinone yield. *Food and Chemical Toxicology*, **39**: 401-406.
- Boese, A. D. (2015). Density Functional Theory and Hydrogen Bonds: Are We There Yet? . *ChemPhysChem*, **16**: 978-985.
- Bolton, J. L., Trush M. A., Penning T. M., Dryhurst G. and Monks T. J. (2000). Role of quinones in toxicology. *Chemical Research in Toxicology*, **13**: 135-160.
- Borgerding, M. and Klus H. (2005). Analysis of complex mixtures—cigarette smoke. *Experimental and Toxicologic Pathology*, **57**: 43-73.

- Busch, C., Streibel T., Liu C., McAdam K. and Zimmermann R. (2012). Pyrolysis and combustion of tobacco in a cigarette smoking simulator under air and nitrogen atmosphere. *Analytical and Bioanalytical Chemistry*, **403**: 419-430.
- Cappelleri, J. , Bushmakina A. , Baker C., Merikle E. , Olufade A. and Gilbert D. (2005). Revealing the multidimensional framework of the Minnesota nicotine withdrawal scale. *Current Medical Research and Opinion*, **21**: 749-760.
- Chalon, S., Moreno H., Benowitz N., Hoffman B. and Blaschke T. (2000). Nicotine impairs endothelium-dependent dilatation in human veins in vivo. *Clinical Pharmacology and Therapeutics*, **67**: 391-397.
- Cho, K., Frijters J. C., Zhang H. , Miller L. L. and Gruen J. R. . (2013). Prenatal Exposure to Nicotine and Impaired Reading Performance. *The Journal of Pediatrics*, **162**: 713-718.
- Christen, A. G., Swanson B. Z., Glover E. D. and Henderson A. H. (1982). Smokeless tobacco: the folklore and social history of snuffing, sneezing, dipping, and chewing. *The Journal of the American Dental Association*, **105**: 821-829.
- Cluette-Brown J. , Mulligan J., Doyle K., Hagan S. , Osmolski T. and Hojnacki J. . (1986). Oral nicotine induces an atherogenic lipoprotein profile. *Proceedings of the Society for Experimental Biology and Medicine*, **182**: 409-413.
- Czégény, Z., Blazsó M., Várhegyi G., Jakab E., Liu C. and Nappi L. (2009). Formation of selected toxicants from tobacco under different pyrolysis conditions. *Journal of Analytical and Applied Pyrolysis*, **85**: 47-53.
- Dellinger, B., Pryor W., Cueto B., Squadrito G. and Deutsch W. (2000). The role of combustion-generated radicals in the toxicity of PM 2.5. *Proceedings of the Combustion Institute*, **28**: 2675-2681.
- Domingo, L. R., Andres J., Moliner V. and Safont V. S. (1997). Theoretical study of the gas phase decomposition of glycolic, lactic, and 2-hydroxyisobutyric acids. *Journal of the American Chemical Society*, **119**: 6415-6422.

- Duncan, J., Garland M. , Myers M. M. , Fifer W. P. , Yang M., Kinney H. C. and Stark R. I. . (2009). Prenatal nicotine-exposure alters fetal autonomic activity and medullary neurotransmitter receptors: implications for sudden infant death syndrome. *Journal of Applied Physiology*, **107**: 1579-1590.
- Elshal, M. F., El-Sayed I. H., Elsaied M. A., El-Masry S. A. and Kumosani T. A. (2009). Sperm head defects and disturbances in spermatozoal chromatin and DNA integrities in idiopathic infertile subjects: association with cigarette smoking. *Clinical biochemistry*, **42**: 589-594.
- Feng, J. W. , Zheng S. K and Maciel G. E. (2004). EPR investigations of charring and char/air interaction of cellulose, pectin, and tobacco. *Energy & Fuels*, **18**: 560-568.
- Forster, M., Liu C., Duke M. G., McAdam K. G. and Proctor C. J. (2015). An experimental method to study emissions from heated tobacco between 100-200 °C. *Chemistry Central Journal*, **9**: 1.
- Foulds, J., Delnevo C., Zeidonis D. and Steinberg M. (2008). Health effects of tobacco, nicotine, and exposure to tobacco smoke pollution. *Handbook of the Medical Consequences of Alcohol and Drug Abuse*: 423-459.
- Frisch, M., Trucks G., Schlegel H. B., Scuseria G. E., Robb M. A., Cheeseman J. R., Montgomery Jr J. A., Vreven T., Kudin K. N. and Burant J. C. (2004). Gaussian 03, revision D. 01. *Gaussian Inc., Wallingford, Connecticut, U.S.A.*
- Frisch, M., Trucks G., Schlegel H., Scuseria G., Robb M., A. and Cheeseman J. (2009). Gaussian 09, Revision B01. *Gaussian Inc., Wallingford Connecticut, U.S.A.*
- Ghosh, A., Choudhury A., Das A., Chatterjee N. S., Das T., Chowdhury R., Panda K., Banerjee R. and Chatterjee I. B. (2012). Cigarette smoke induces p-benzoquinone–albumin adduct in blood serum: implications on structure and ligand binding properties. *Toxicology*, **292**: 78-89.
- Gori, G., Benowitz N. and Lynch C. (1986). Mouth versus deep airways absorption of nicotine in cigarette smokers. *Pharmacology Biochemistry and Behaviour*, **25**: 1181-1184.

- Hanulikova, B., Kuritka I. and Urbanek P. (2016). Effect of backbone conformation and its defects on electronic properties and assessment of the stabilizing role of  $\pi$ - $\pi$  interactions in aryl substituted polysilylenes studied by DFT on deca [methyl (phenyl) silylene] s. *Chemistry Central Journal*, **10**: 1-4.
- Hecht, S. (2005). Carcinogenicity studies of inhaled cigarette smoke in laboratory animals: old and new. *Carcinogenesis*, **26**: 1488-1492.
- Henningfield, J. and Keenan R. (1993). Nicotine delivery kinetics and abuse liability. *Journal of Consulting and Clinical Psychology*, **61**: 743-750.
- Hesami, Z., Alvanpour A., Kashani B. S, Tafti S. F. and Reza G. (2010). Severity of Nicotine Withdrawal Symptoms after Smoking Cessation. *Tanaffos*, **9**: 42-47.
- Hetch, S. (2012). Lung carcinogenesis by tobacco smoke. *International Journal of Cancer*, **131**: 2724-2732.
- Hinchliffe, A. (2005). *Molecular Modelling for Beginners*. Hoboken, New Jersey, USA: John Wiley & Sons.
- Huang, M., Choi S., Kim D., Kim D., Bae H., Yu S. and Park J. . (2011). Evaluation of Factors Associated with Cadmium Exposure and Kidney Function in the General Population. *Wiley Periodicals, Inc.*: 563-570.
- Hukkanen, J., Jacob P. and Benowitz N. L. (2005). Metabolism and Disposition Kinetics of Nicotine. *Pharmacological Review*, **57**: 79-115.
- Jha, P., Ramasundarahettige C., Landsman V., Rostron B., Thun M., Anderson R. , McAfee T. and Peto R. (2013). 21st-century hazards of smoking and benefits of cessation in the United States. *New England Journal of Medicine*, **368**: 341-350.
- Kibet, J. K., Mathenge A. B., Kituyi L. and Okumu T. (2014). The Product Distribution and Molecular Modeling of Ethyl Benzene and Toluene. *The Journal of Kenya Chemical Society Volume 8: Issue, 8*: 63-68.
- Kibet, J., Khachatryan L. and Dellinger B. (2012). Molecular Products and Radicals from Pyrolysis of Lignin. *Environmental science & technology*, **46**: 12994-13001.

- Kulshreshtha, N. P. and Moldoveanu S. C. (2003). Analysis of pyridines in mainstream cigarette smoke. *Journal of Chromatography A*, **985**: 303-312.
- Lenoid, S. (2012). Chemissian v3.3.
- Leshner, A. I. (1998). Drug addiction research: moving toward the 21st century. *Drug and alcohol dependence*, **51**: 5-7.
- Lisko, J., Stanfill S. B., Duncan B. W. and Watson C. H. (2013). Application of GC-MS/MS for the analysis of tobacco alkaloids in cigarette filler and various tobacco species. *Analytical Chemistry*, **85**: 3380-3384.
- Liu, X., Castagnoli K., Van der Schyf C. J. and Castagnoli N. (2000). Studies on the in vivo biotransformation of the tobacco alkaloid  $\beta$ -nicotyrine. *Chemical Research in Toxicology*, **13**: 336-341.
- Ljungberg, L. , Persson K. , Eriksson A., Green H. and Whiss P. (2013). Effects of nicotine, its metabolites and tobacco extracts on human platelet function in vitro. *Toxicology in Vitro*, **27**: 932-938.
- Lockman, P. R., McAfee G., Geldenhuys W. J., Van der Schyf C. J., Abbruscato T. J. and Allen D. D. (2005). Brain uptake kinetics of nicotine and cotinine after chronic nicotine exposure. *The journal of pharmacology and experimental therapeutics*, **314**: 216-230.
- McQuarrie, D. A. and Simon J. D. (1997). *Physical chemistry: a molecular approach* (Vol. 1). Sausalito, CA, USA: Sterling Publishing Company.
- Mendelsohn C. (2011). Nicotine dependence: why is it so hard to quit? *Medicine Today*, **12**: 35-40.
- Mitschke, S. , Adam T., Streibel T. , Baker R. R. and Zimmermann R. (2005). Application of time-of-flight mass spectrometry with laser-based photoionization methods for time-resolved on-line analysis of mainstream cigarette smoke. *Analytical Chemistry*, **77**: 2288-2296.

- Mwenda, S. N., Wanjoya A. K. and Waititu A. G. (2015). Analysis of Tobacco Smoking Patterns in Kenya using the Multinomial Logit Model. *American Journal of Theoretical and Applied Statistics*, **4**: 89-98.
- Nadendla, R. R. (2004). Molecular modeling: A powerful tool for drug design and molecular docking. *Resonance*, **9**: 51-60.
- Neha, G. and Derek D. R. (2010). A transport model for nicotine in the tracheobronchial and pulmonary region of the lung. *Inhalation Toxicology*, **22**: 42-48.
- Nganai, S., Lomnicki S. and Dellinger B. (2012). Formation of PCDD/Fs from oxidation of 2-monochlorophenol over an Fe<sub>2</sub>O<sub>3</sub>/silica surface. *Chemosphere*, **88**: 371-376.
- Ochterski, J. W. (2000). Thermochemistry in gaussian. *Gaussian Inc, Pittsburgh, Pennsylvania, USA*: 1-17.
- Osorio, E., Vasquez A., Florez E., Mondragon F., Donald K. J. and Tiznado W. (2013). Theoretical design of stable small aluminium-magnesium binary clusters. *Physical Chemistry Chemical Physics*, **15**: 2222-2229.
- Pankow, J. (2001). A consideration of the role of gas/particle partitioning in the deposition of nicotine and other tobacco smoke compounds in the respiratory tract. *Chemical Research in Toxicology*, **14**: 1465-1481.
- Pérez, P. V. , Travieso D. H., Roche R. G., Gorbea B. G., Pérez T. R. and Fernández S. J. (2009). Smoking-Attributable Mortality in Cuba. *MEDICC Review*, **11**: 43-47.
- Pomerleau, O. .F and Rosecrans J. (1989). Neuroregulatory effects of nicotine. *Psychoneuroendocrinology*, **14**: 407-423.
- Robson, N., Bond A. J. and Wolff K. . (2010). Salivary nicotine and cotinine concentrations in unstimulated and stimulated saliva. *African Journal of Pharmacy and Pharmacology*, **4**: 061-065.
- Sadeu, J. C., Hughes C. L., Agarwal S. and Foster W. G. (2010). Alcohol, drugs, caffeine, tobacco, and environmental contaminant exposure: reproductive health consequences and clinical implications. *Critical reviews in toxicology*, **40**: 633-652.

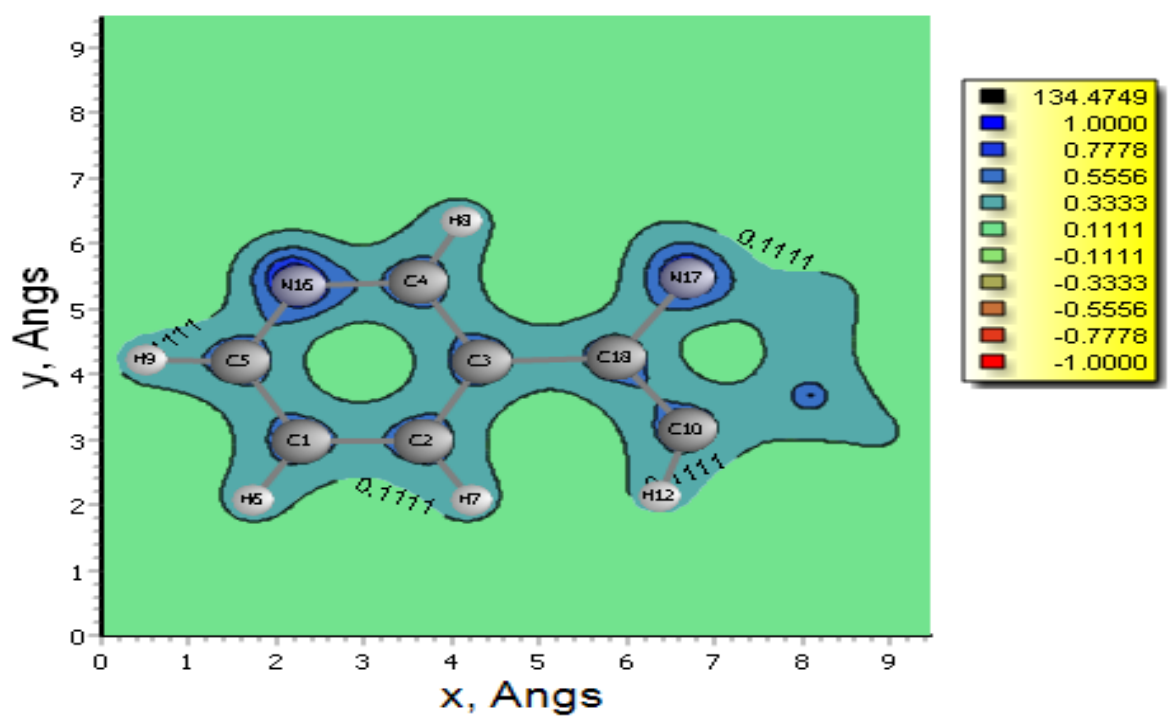
- Schlotzhauer, W. (1982). Pyrolytic Studies on the contribution of tobacco leaf constituents to the formation of smoke catechols. *Agriculture and Food Chemistry*, **30**: 372-374.
- Sharma, R. K. and Hajaligol M. R. . (2003). Effect of pyrolysis conditions on the formation of polycyclic aromatic hydrocarbons (PAHs) from polyphenolic compounds. *Journal of Analytical and Applied Pyrolysis*, **66**: 123-144.
- Sharma, R. K., Wooten J. B., Baliga V. L., Lin X., Chan W. G. and Hajaligol M. R. (2004). Characterization of chars from pyrolysis of lignin. *Fuel*, **83**: 1469-1482.
- Shaywitz, S. E. and Shaywitz B. A. (1996). Unlocking learning disabilities: The neurological basis. *Learning disabilities: Lifelong issues. Baltimore, Maryland, USA : PH Brooks Publishing*: 255-260.
- Shiffman, S., Ferguson S. G., Gwaltney C. J., Balabanis M. H. and Shadel W. G. (2006). Reduction of abstinence-induced withdrawal and craving using high-dose nicotine replacement therapy. *Psychopharmacology*, **184**: 637-644.
- Siegel, R., Naishadham D. and Jemal A. (2012). Cancer Statistics. *Cancer Journal of Clinicians*, **62**: 10-29.
- Stedman, R. (1968). The chemical composition of tobacco and tobacco smoke. *Chemical Reviews*, **68**: 153-207.
- Strohschneider, T., Oberhoff M., Hanke H., Hannekum A. and Karsch K. (1994). Effect of chronic nicotine delivery on the proliferation rate of endothelial and smooth muscle cells in experimentally induced vascular wall plaques. *Journal of Clinical investigation*, **72**: 908-912.
- Talhout, R. , Opperhuizen A. and Amsterdam J. G. (2006). Sugars as tobacco ingredient: Effects on mainstream smoke composition. *Food and Chemical Toxicology*, **44**: 1789-1798.
- Talikka, M., Sierro N., Ivanov N. V., Chaudhary N., Peck M. J., Hoeng J., Coggins C. R. and Peitsch M. C. (2012). Genomic impact of cigarette smoke, with application to three smoking-related diseases. *Critical reviews in toxicology*, **42**: 877-889.

- Taylor, P., Dellinger B. and Lee C. C. (1990). Development of a thermal stability-based ranking of hazardous organic compound incinerability. *Environmental science & technology*, **24**: 316-328.
- Uddin, K. M., Warburton P. L. and Poirier R. A. (2012). Comparisons of Computational and Experimental Thermochemical Properties of alpha-Amino Acids. *Journal of Physical Chemistry B*, **116**: 3220-3234.
- W.H.O. (2011). *World Health Organization report on the global tobacco epidemic, 2011: warning about the dangers of tobacco*: Geneva: World Health Organization.
- Wang, S. R., Guo X. J., Liang T., Zhou Y. and Luo Z. Y. (2012). Mechanism research on cellulose pyrolysis by Py-GC/MS and subsequent density functional theory studies. *Bioresource Technology*, **104**: 722-728.
- Wang, Z., Koenig H. G. and Al Shohaib S. (2015). Religious involvement and tobacco use in mainland China: a preliminary study. *BMC Public Health*, **15**: 1-8.
- Wetter, D. W., Kenford S. L. , Smith S. S., Fiore M. C., Jorenby D. E. and Baker T. B. . (1999). Gender Differences in Smoking Cessation. *Journal of Consulting and Clinical Psychology*, **67**: 555-562.
- White, J. E., Catallo W. J. and Legendre B. L. (2011). Biomass pyrolysis kinetics: A comparative critical review with relevant agricultural residue case studies. *Journal of Analytical and Applied Pyrolysis*, **91**: 1-33.
- William, W., Daisy Su D. and Yuan J. (2012). Cigarette smoking in China: public health, science, and policy. *Reviews on Environmental Health*, **27**: 43-49.
- Wójcik, J., Peszke J., Ratuszna A., Kuś P. and Wrzalik R. (2013). Theoretical investigation of porphyrin-based photosensitizers with enhanced NIR absorption. *Physical Chemistry Chemical Physics*, **15**: 19651-19658.
- Young, C. D. (2001). *Computational Chemistry: A Practical Guide for Applying Techniques to Real-World Problems*. John Wiley & Sons, Inc.: 1-398.

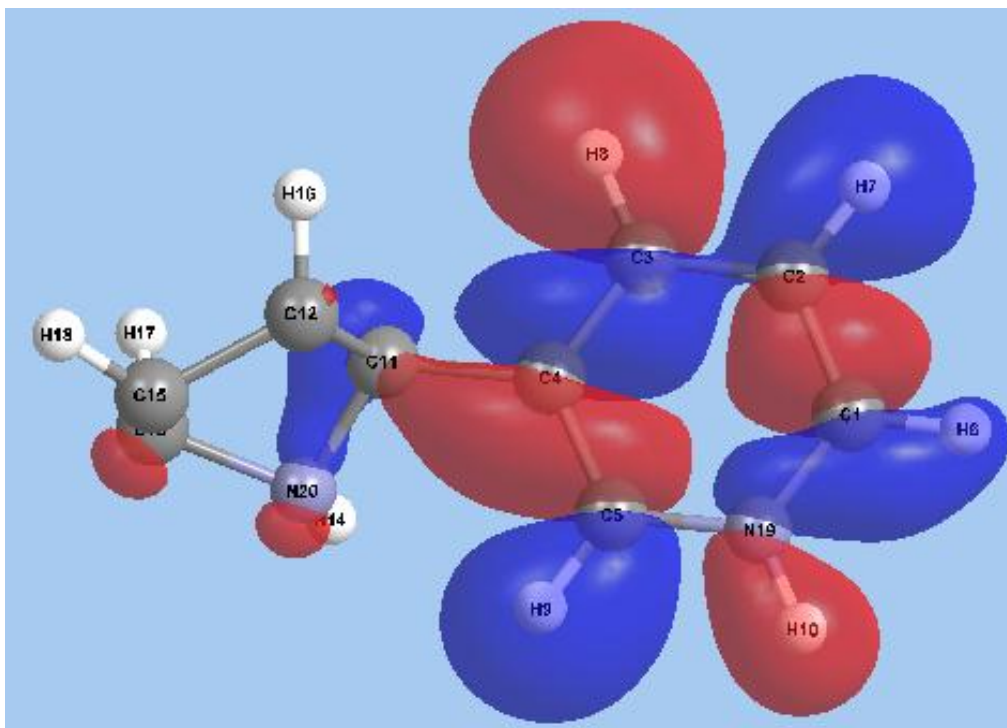
- Zhang, X., Yang W. and Blasiak W. (2012). Kinetics of levoglucosan and formaldehyde formation during cellulose pyrolysis process. *Energy & Fuels*, **96**: 383-391.
- Zhang, Z., Lin L. and Wang L. (2012). Atmospheric oxidation mechanism of naphthalene initiated by OH radical. A theoretical study. *Physical Chemistry Chemical Physics*, **14**: 2645-2650.
- Zhao, Ford E. S., Tsai J., Li C., Ahluwalia I. B., Pearson W. S., Balluz L. S. and Croft J. B. (2012). Trends in health-related behavioral risk factors among pregnant women in the United States: 2001–2009. *Journal of Women's Health*, **21**: 255-263.
- Zhao, Ford E., Tsai J., Li C., Ahluwalia I. and Pearson W. . (2012). Trends in health-related behavioral risk factors among pregnant women in the United States: 2001–2009. *Journal of Women's Health*, **21**: 255-263.
- Zhou, S., Wang C., Xu Y. and Hu Y. (2011). The pyrolysis of cigarette paper under the conditions that simulate cigarette smouldering and puffing. *Journal of thermal analysis and calorimetry*, **104**: 1097-1106.

## APPENDICES

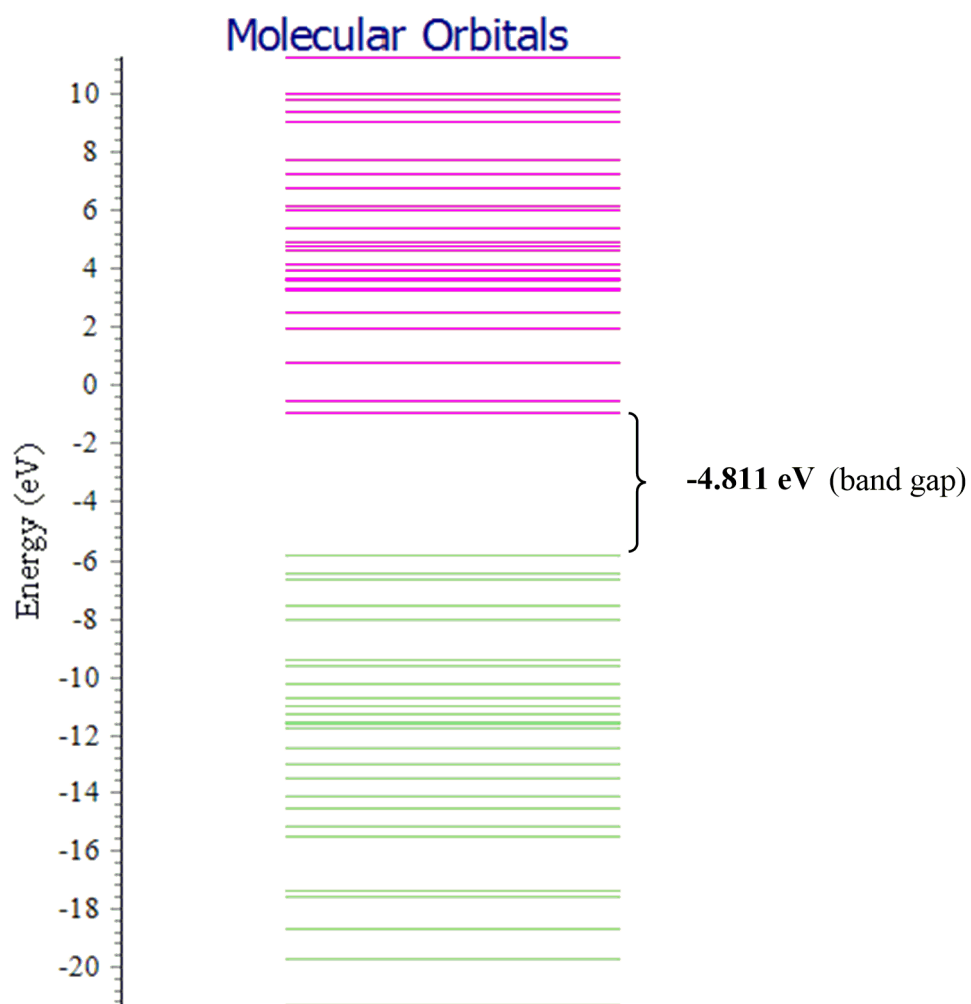
Appendix 1A: 2-D electron density contour map for  $\beta$ -nicotyrine



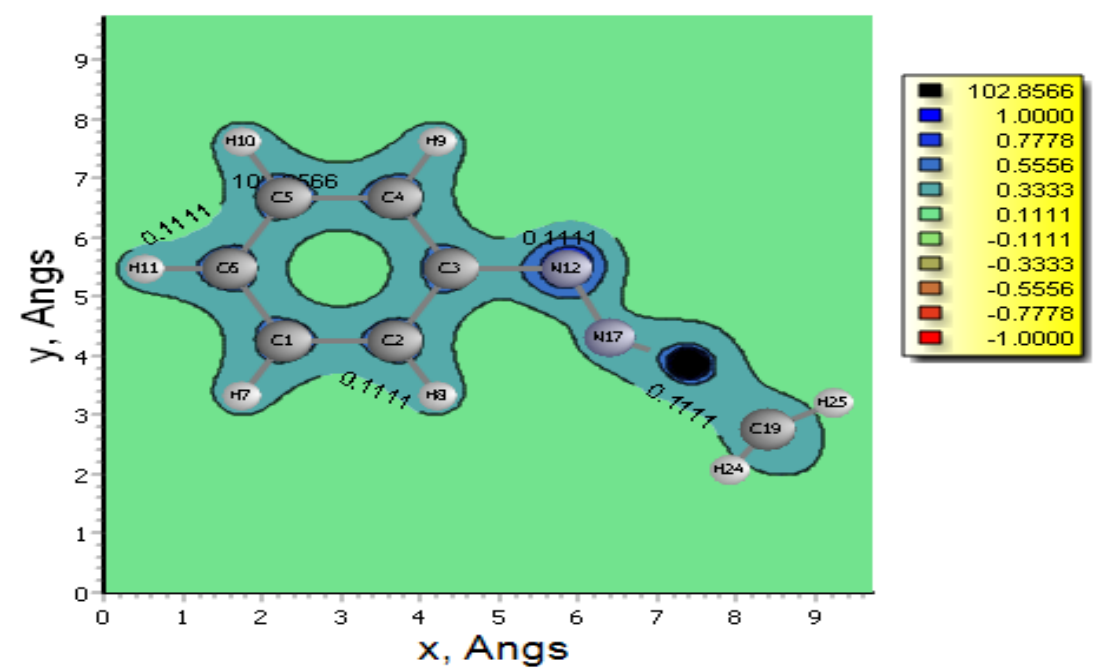
**Appendix 1B:** 3-D electron density map for  $\beta$ -nicotyrine



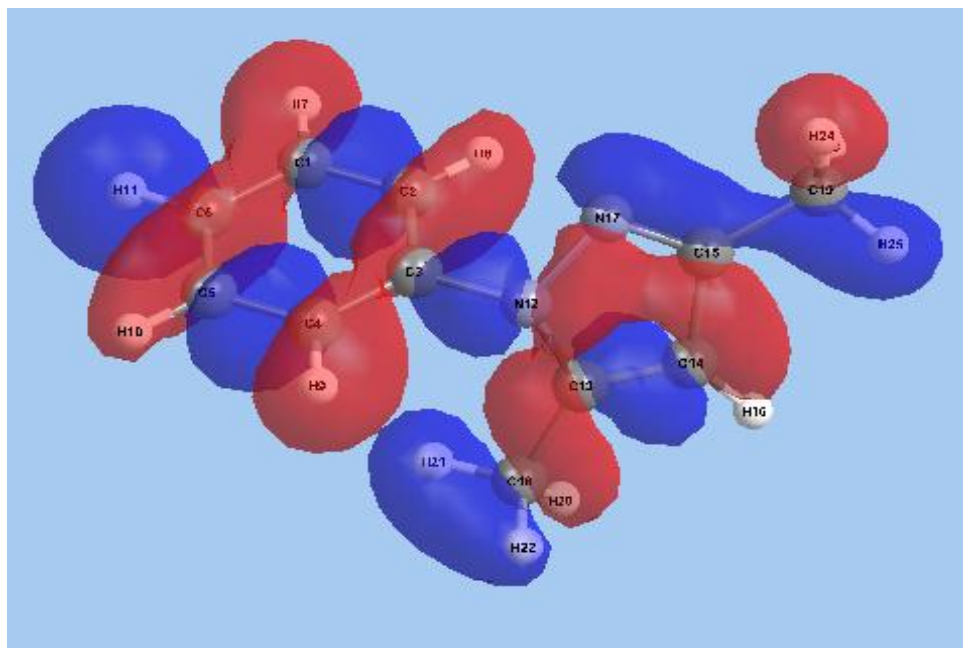
**Appendix 1C:** Molecular orbital diagram for  $\beta$ -nicotyrine



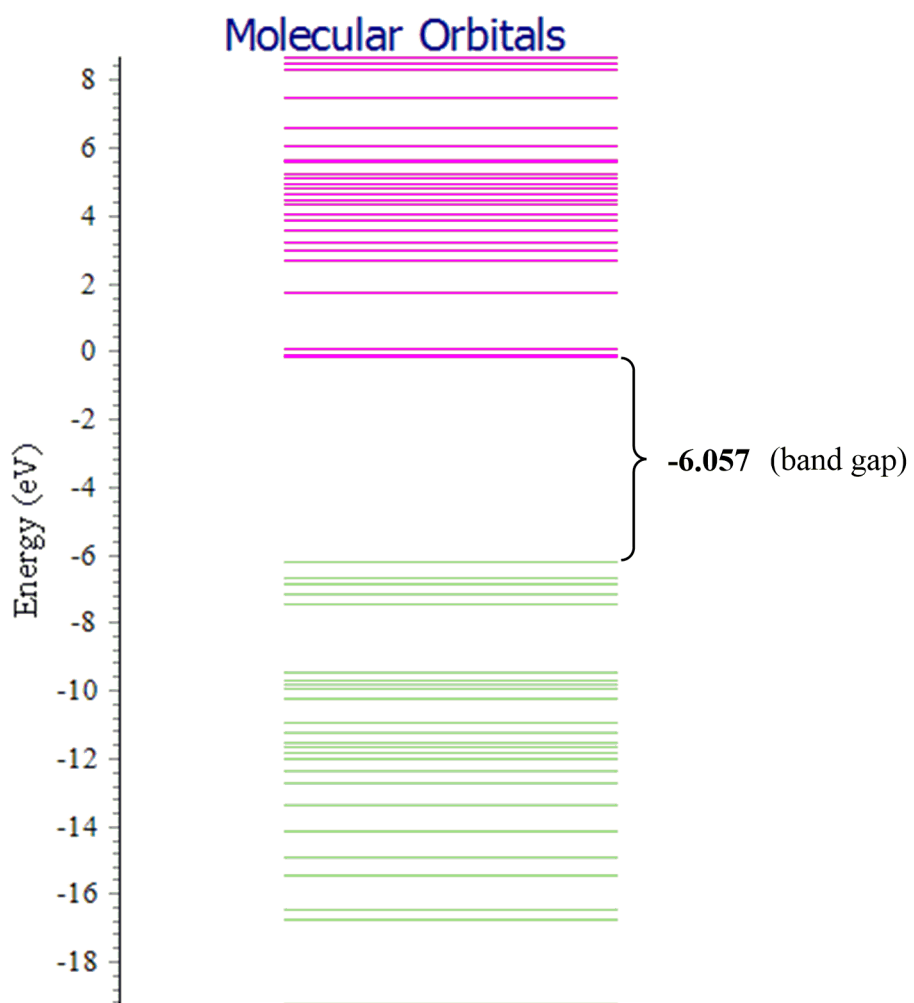
**Appendix 2A:** 2-D electron density contour map for 3, 5-dimethyl-1-phenylpyrazole



**Appendix 2B:** 3-D electron density map for 3,5-dimethyl-1-phenylpyrazole



**Appendix 2C:** Molecular orbital diagram for 3, 5-dimethyl-1-phenylpyrazole



### Appendix 3: Frequency and thermochemistry output file for optimization of pyridinyl radical

Full mass-weighted force constant matrix:

Low frequencies --- -19.1100 -13.9534 -0.0009 -0.0007 -0.0003 2.0451

Low frequencies --- 399.0217 438.0293 595.5201

Diagonal vibrational polarizability:

1.1043663 1.5610057 3.6797222

Harmonic frequencies (cm<sup>-1</sup>), IR intensities (KM/Mole), Raman scattering activities (A<sup>4</sup>/AMU), depolarization ratios for plane and unpolarized incident light, reduced masses (AMU), force constants (mDyne/A), and normal coordinates:

	1	2	3
	A	A	A
Frequencies --	399.0212	438.0291	595.5201
Red. masses --	2.7803	4.2158	7.8729
Frc consts --	0.2608	0.4766	1.6450
IR Inten --	2.8698	0.0063	18.7184

Atom AN	X	Y	Z	X	Y	Z	X	Y	Z
1 6	0.00	0.00	0.24	0.00	0.00	-0.04	0.17	0.23	0.00
2 6	0.00	0.00	-0.12	0.00	0.00	0.24	-0.30	0.27	0.00
3 6	0.00	0.00	-0.13	0.00	0.00	-0.33	-0.18	-0.13	0.00
4 6	0.00	0.00	0.21	0.00	0.00	0.00	-0.18	-0.18	0.00
5 6	0.00	0.00	-0.12	0.00	0.00	-0.21	0.15	0.10	0.00
6 1	0.00	0.00	0.56	0.00	0.00	0.03	0.28	-0.01	0.00
7 1	0.00	0.00	-0.27	0.00	0.00	0.71	-0.34	0.22	0.00
8 1	0.00	0.00	0.59	0.00	0.00	0.15	-0.30	0.14	0.00
9 1	0.00	0.00	-0.33	0.00	0.00	-0.45	-0.22	0.13	0.00
10 7	0.00	0.00	-0.11	0.00	0.00	0.26	0.34	-0.28	0.00

	4	5	6
	A	A	A
Frequencies --	675.1487	704.6629	803.3418
Red. masses --	7.2797	2.2120	1.5116

Frc consts --	1.9551	0.6471	0.5748
IR Inten --	2.7961	34.3180	31.0437
Atom AN	X Y Z	X Y Z	X Y Z
1 6	0.33 0.01 0.00	0.00 0.00 -0.15	0.00 0.00 0.04
2 6	0.14 0.09 0.00	0.00 0.00 0.07	0.00 0.00 0.12
3 6	-0.02 0.43 0.00	0.00 0.00 -0.12	0.00 0.00 -0.10
4 6	-0.31 -0.04 0.00	0.00 0.00 0.12	0.00 0.00 0.08
5 6	0.03 -0.34 0.00	0.00 0.00 0.13	0.00 0.00 0.09
6 1	0.22 0.25 0.00	0.00 0.00 0.08	0.00 0.00 -0.75
7 1	-0.14 -0.29 0.00	0.00 0.00 0.51	0.00 0.00 -0.51
8 1	-0.25 -0.20 0.00	0.00 0.00 0.49	0.00 0.00 -0.15
9 1	-0.03 -0.34 0.00	0.00 0.00 0.62	0.00 0.00 -0.34
10 7	-0.13 -0.09 0.00	0.00 0.00 -0.17	0.00 0.00 -0.07
	7	8	9
	A	A	A
Frequencies --	937.2052	962.4442	992.1842
Red. masses --	1.3440	1.3482	8.6355
Frc consts --	0.6955	0.7358	5.0087
IR Inten --	0.7314	0.2507	5.3297
Atom AN	X Y Z	X Y Z	X Y Z
1 6	0.00 0.00 0.03	0.00 0.00 0.03	0.42 0.14 0.00
2 6	0.00 0.00 0.06	0.00 0.00 -0.10	-0.07 0.09 0.00
3 6	0.00 0.00 0.02	0.00 0.00 0.02	-0.04 -0.43 0.00
4 6	0.00 0.00 -0.15	0.00 0.00 -0.07	0.02 -0.11 0.00
5 6	0.00 0.00 -0.04	0.00 0.00 0.12	0.08 -0.02 0.00
6 1	0.00 0.00 -0.21	0.00 0.00 -0.29	0.53 -0.06 0.00
7 1	0.00 0.00 -0.38	0.00 0.00 0.58	-0.07 0.07 0.00
8 1	0.00 0.00 0.84	0.00 0.00 0.39	0.05 -0.20 0.00
9 1	0.00 0.00 0.27	0.00 0.00 -0.63	0.13 -0.02 0.00
10 7	0.00 0.00 0.03	0.00 0.00 -0.01	-0.39 0.30 0.00
	10	11	12
	A	A	A
Frequencies --	1012.9335	1054.4541	1075.7611

Red. masses --	1.4252	4.9885	2.0287
Frc consts --	0.8616	3.2680	1.3832
IR Inten --	0.3689	3.0776	6.8617
Atom AN	X Y Z	X Y Z	X Y Z
1 6	0.00 0.00 -0.14	0.09 0.05 0.00	0.04 -0.06 0.00
2 6	0.00 0.00 0.08	0.25 -0.27 0.00	-0.14 0.00 0.00
3 6	0.00 0.00 0.00	-0.02 -0.02 0.00	0.03 0.16 0.00
4 6	0.00 0.00 -0.04	-0.25 -0.10 0.00	0.13 -0.08 0.00
5 6	0.00 0.00 0.11	-0.02 0.38 0.00	0.00 0.12 0.00
6 1	0.00 0.00 0.69	0.16 -0.03 0.00	0.27 -0.55 0.00
7 1	0.00 0.00 -0.41	0.13 -0.45 0.00	-0.37 -0.30 0.00
8 1	0.00 0.00 0.13	-0.30 -0.01 0.00	0.27 -0.46 0.00
9 1	0.00 0.00 -0.55	-0.34 0.42 0.00	-0.11 0.13 0.00
10 7	0.00 0.00 0.00	-0.01 -0.04 0.00	-0.06 -0.03 0.00

13 14 15

A A A

Frequencies --	1121.9766	1219.5640	1276.2711
Red. masses --	2.0586	1.2864	5.3813
Frc consts --	1.5268	1.1273	5.1644
IR Inten --	1.0375	2.2694	0.9345

Atom AN	X Y Z	X Y Z	X Y Z
1 6	0.09 0.12 0.00	-0.04 0.02 0.00	-0.11 0.17 0.00
2 6	-0.04 -0.11 0.00	-0.02 0.00 0.00	-0.12 -0.13 0.00
3 6	-0.03 -0.03 0.00	0.00 0.01 0.00	0.18 -0.02 0.00
4 6	0.13 0.16 0.00	0.00 -0.12 0.00	-0.12 0.22 0.00
5 6	-0.07 -0.04 0.00	0.05 0.02 0.00	0.34 0.04 0.00
6 1	-0.06 0.46 0.00	-0.31 0.58 0.00	-0.04 0.01 0.00
7 1	-0.37 -0.56 0.00	-0.30 -0.38 0.00	0.16 0.25 0.00
8 1	0.12 0.19 0.00	0.05 -0.26 0.00	0.09 -0.39 0.00
9 1	-0.43 -0.03 0.00	0.48 0.00 0.00	0.61 0.01 0.00
10 7	0.00 -0.08 0.00	0.02 0.07 0.00	-0.21 -0.23 0.00

16 17 18

A A A

Frequencies --	1361.6780	1453.0787	1480.5391
Red. masses --	1.2795	1.8971	1.7449
Frc consts --	1.3978	2.3600	2.2535
IR Inten --	1.7391	19.1404	6.2261
Atom AN	X Y Z	X Y Z	X Y Z
1 6	-0.04 0.00 0.00	-0.09 0.01 0.00	0.02 -0.06 0.00
2 6	0.01 0.07 0.00	-0.01 0.04 0.00	-0.11 -0.06 0.00
3 6	0.12 -0.02 0.00	0.14 -0.06 0.00	0.06 0.08 0.00
4 6	-0.02 -0.02 0.00	-0.12 0.03 0.00	0.05 -0.12 0.00
5 6	-0.02 0.00 0.00	0.09 -0.07 0.00	0.12 0.03 0.00
6 1	0.09 -0.28 0.00	-0.04 -0.14 0.00	-0.21 0.41 0.00
7 1	-0.34 -0.40 0.00	-0.26 -0.29 0.00	0.15 0.30 0.00
8 1	-0.28 0.68 0.00	0.02 -0.37 0.00	-0.20 0.56 0.00
9 1	0.28 -0.02 0.00	-0.78 -0.04 0.00	-0.51 0.06 0.00
10 7	-0.04 -0.02 0.00	0.06 0.11 0.00	-0.06 0.03 0.00
	19	20	21
	A	A	A

Frequencies --	1545.9227	1612.2957	3200.3479
Red. masses --	4.7784	6.0946	1.0860
Frc consts --	6.7283	9.3344	6.5534
IR Inten --	7.2771	7.1928	1.1564
Atom AN	X Y Z	X Y Z	X Y Z
1 6	-0.09 0.38 0.00	-0.21 0.11 0.00	-0.05 -0.03 0.00
2 6	-0.07 -0.28 0.00	0.28 0.12 0.00	0.04 -0.02 0.00
3 6	0.01 0.10 0.00	-0.37 0.02 0.00	0.00 0.00 0.00
4 6	0.03 -0.18 0.00	0.17 -0.09 0.00	0.00 0.00 0.00
5 6	-0.05 -0.16 0.00	0.33 -0.04 0.00	0.00 0.04 0.00
6 1	0.37 -0.57 0.00	-0.02 -0.36 0.00	0.64 0.30 0.00
7 1	0.26 0.14 0.00	-0.10 -0.40 0.00	-0.41 0.30 0.00
8 1	-0.09 0.18 0.00	0.07 0.22 0.00	-0.02 -0.01 0.00
9 1	0.19 -0.19 0.00	-0.43 -0.03 0.00	-0.03 -0.47 0.00
10 7	0.09 0.15 0.00	-0.14 -0.06 0.00	0.00 0.00 0.00
	22	23	24

	A			A			A		
Frequencies --	3211.9845			3226.3963			3237.3069		
Red. masses --	1.0908			1.0971			1.0929		
Frc consts --	6.6301			6.7287			6.7483		
IR Inten --	15.7632			23.5847			5.5702		
Atom AN	X	Y	Z	X	Y	Z	X	Y	Z
1 6	0.00	-0.01	0.00	-0.06	-0.03	0.00	0.01	0.01	0.00
2 6	-0.05	0.04	0.00	-0.03	0.03	0.00	0.01	-0.01	0.00
3 6	0.00	0.00	0.00	0.00	0.00	0.00	0.00	0.00	0.00
4 6	0.00	0.00	0.00	-0.02	-0.01	0.00	-0.08	-0.03	0.00
5 6	0.00	0.06	0.00	0.00	-0.05	0.00	0.00	0.02	0.00
6 1	0.07	0.04	0.00	0.61	0.28	0.00	-0.15	-0.07	0.00
7 1	0.59	-0.44	0.00	0.34	-0.26	0.00	-0.09	0.07	0.00
8 1	-0.02	-0.01	0.00	0.25	0.09	0.00	0.90	0.33	0.00
9 1	-0.04	-0.67	0.00	0.02	0.53	0.00	-0.01	-0.18	0.00
10 7	0.00	0.00	0.00	0.00	0.00	0.00	0.00	0.00	0.00

-----

- Thermochemistry -

-----

Temperature 298.15 Kelvin. Pressure 1.00000 Atm.

Atom 1 has atomic number 6 and mass 12.00000

Atom 2 has atomic number 6 and mass 12.00000

Atom 3 has atomic number 6 and mass 12.00000

Atom 4 has atomic number 6 and mass 12.00000

Atom 5 has atomic number 6 and mass 12.00000

Atom 6 has atomic number 1 and mass 1.00783

Atom 7 has atomic number 1 and mass 1.00783

Atom 8 has atomic number 1 and mass 1.00783

Atom 9 has atomic number 1 and mass 1.00783

Atom 10 has atomic number 7 and mass 14.00307

Molecular mass: 78.03437 amu.

Principal axes and moments of inertia in atomic units:

	1	2	3
EIGENVALUES --	277.86089	314.48935	592.35024
X	0.98548	0.16979	0.00000
Y	-0.16979	0.98548	0.00000
Z	0.00000	0.00000	1.00000

This molecule is an asymmetric top.

Rotational symmetry number 1.

Rotational temperatures (Kelvin) 0.31172 0.27541 0.14622

Rotational constants (GHZ): 6.49512 5.73864 3.04675

Zero-point vibrational energy 200961.1 (Joules/Mol)  
48.03085 (Kcal/Mol)

Warning -- explicit consideration of 13 degrees of freedom as  
vibrations may cause significant error

Vibrational temperatures: 574.10 630.23 856.82 971.39 1013.85  
(Kelvin) 1155.83 1348.43 1384.74 1427.53 1457.38  
1517.12 1547.78 1614.27 1754.68 1836.27  
1959.15 2090.65 2130.16 2224.24 2319.73  
4604.58 4621.32 4642.06 4657.76

Zero-point correction= 0.076542 (Hartree/Particle)

Thermal correction to Energy= 0.090828

Thermal correction to Enthalpy= 0.092642

Thermal correction to Gibbs Free Energy= 0.014561

Sum of electronic and zero-point Energies= -247.450049

Sum of electronic and thermal Energies= -247.435763

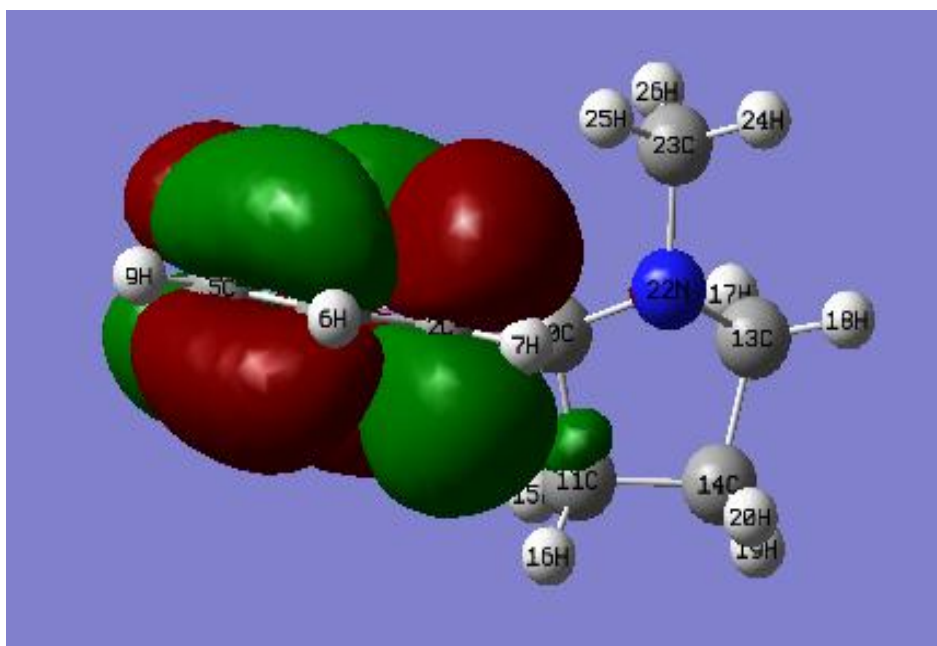
Sum of electronic and thermal Enthalpies= -247.433948

Sum of electronic and thermal Free Energies= -247.512029

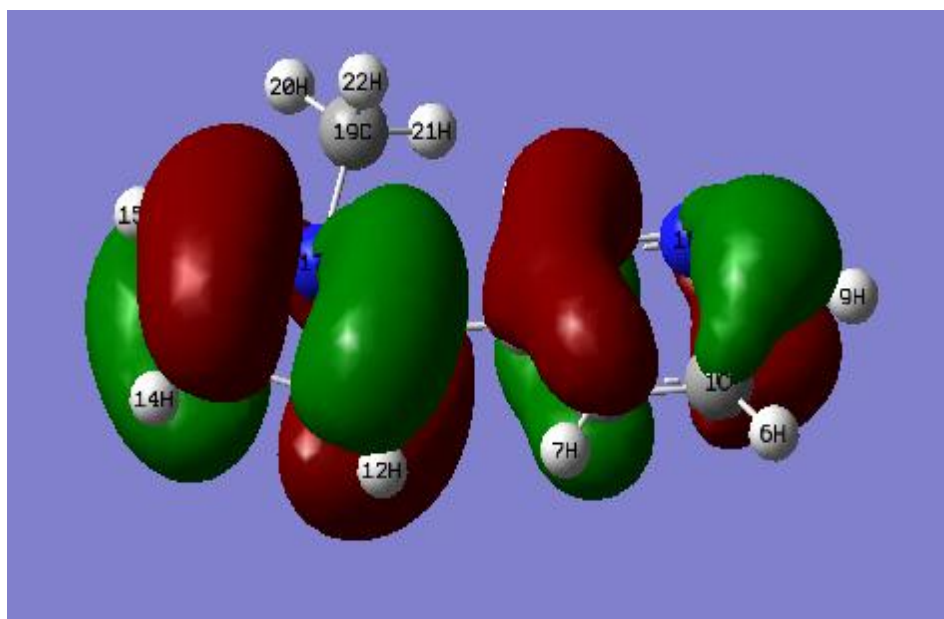
	E (Thermal)	CV	S
	KCal/Mol	Cal/Mol-Kelvin	Cal/Mol-Kelvin
Total	56.995	29.537	85.509
Electronic	0.000	0.000	1.377
Translational	1.708	2.981	42.224

Rotational	1.708	2.981	27.399
Vibrational	53.579	23.575	14.508

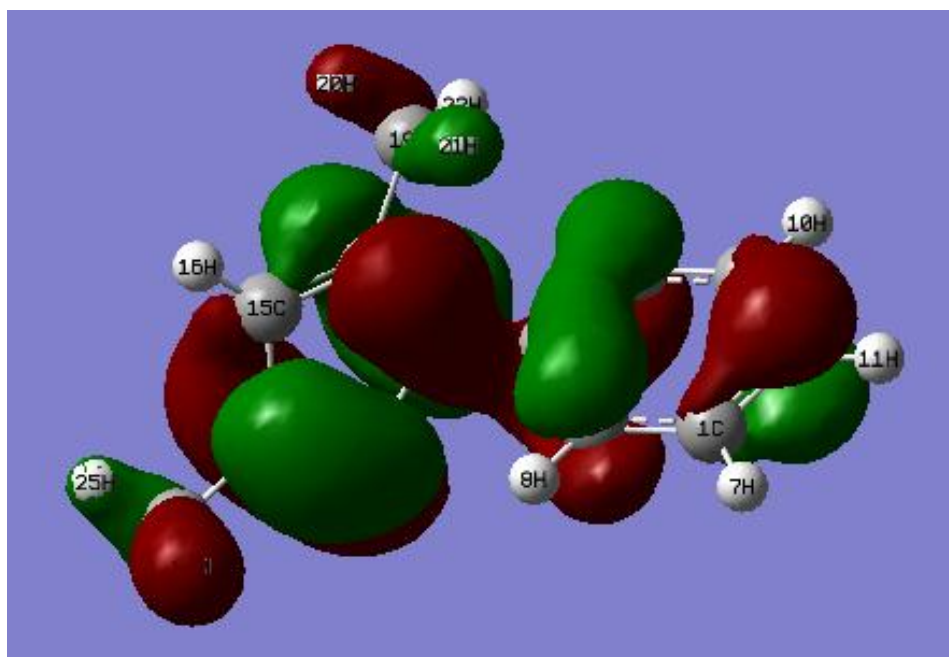
**Appendix 4A:** Molecular orbital diagrams for nicotine



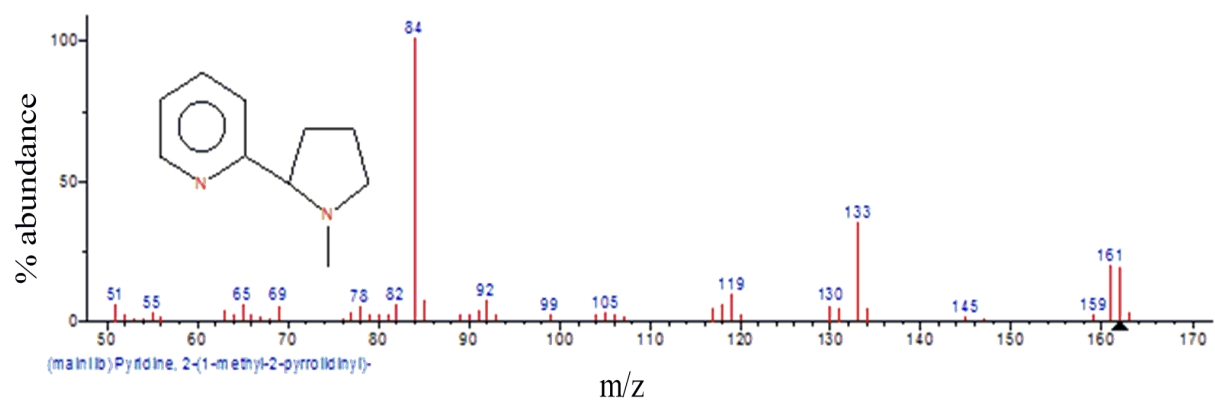
**Appendix 4B:** Molecular orbital diagrams for  $\beta$ -nicotyrine



**Appendix 4C:** Molecular orbital diagrams for 3,5-dimethyl-1-phenylpyrazole



### Appendix 5A: MS-Fragmentation pattern of nicotine using Electron Impact Ionization (EI)



**Appendix 5B:** MS-Fragmentation pattern of  $\beta$ -nicotyrine using Electron Impact Ionization (EI)

